

Article

Wave Height Reduction Inside Pohang New Port, Korea, Due to the Construction of a Detached Breakwater

Kyong Ho Ryu, Weon Mu Jeong , Jung-Eun Oh, Won-Dae Baek and Yeon S. Chang *

Maritime ICT R & D Center, Korea Institute of Ocean Science and Technology, Busan 49111, Korea

* Correspondence: yeonschang@kiost.ac.kr; Tel.: +82-51-664-3566

Abstract: The effect of a detached breakwater, which was constructed to improve harbor tranquility inside Pohang New Port, was examined through the comparison of wave data measured before and after the construction of the breakwater. The observation data showed that the wave energy was effectively reduced by the breakwater, although the wave height measured outside the breakwater was higher after its construction. The wave energy was reduced in all of the measured wave-propagating directions, but it was also observed that the breakwater became less effective in protecting against northeastwaves than in protecting against NNE waves. The BOUSS-2D Boussinesq-type wave model was employed to analyze the pattern of wave propagation, showing that, before the breakwater's construction, NE waves could directly enter the port, increasing the wave energy inside the port. After the breakwater's construction, simulations showed that the detached breakwater effectively blocked the waves approaching the port from both the NNE and NE directions, although the wave heights of the waves from the extreme NE direction inside the port increased. Considering that the estimated probability of failing to preserve the port tranquility was only 0.2–0.5% for these extreme NE waves, it was concluded that no secondary structures were necessary, and the existing breakwater was sufficient for the protection of the port.

Keywords: detached breakwater; port protection; harbor tranquility; BOUSS-2D; Pohang New Port



Citation: Ryu, K.H.; Jeong, W.M.; Oh, J.-E.; Baek, W.-D.; Chang, Y.S. Wave Height Reduction Inside Pohang New Port, Korea, Due to the Construction of a Detached Breakwater. *J. Mar. Sci. Eng.* **2022**, *10*, 1537. <https://doi.org/10.3390/jmse10101537>

Academic Editors: Maria Teresa Reis, João Alfredo Santos and Tiago Fazeres Ferradosa

Received: 17 September 2022

Accepted: 18 October 2022

Published: 19 October 2022

Publisher's Note: MDPI stays neutral with regard to jurisdictional claims in published maps and institutional affiliations.



Copyright: © 2022 by the authors. Licensee MDPI, Basel, Switzerland. This article is an open access article distributed under the terms and conditions of the Creative Commons Attribution (CC BY) license (<https://creativecommons.org/licenses/by/4.0/>).

1. Introduction

Since the construction of Pohang New Port inside Yeongil Bay in the southeastern end of the Korean Peninsula in 1985, questions have been raised regarding the harbor's tranquility because downtime occurs frequently, which might lower the port's operation rate. Unexpected downtime due to harbor agitation may interrupt port operation and reduce throughput, and harbors with complex topologies and layouts are prone to experiencing severe agitation and downtime problems that are difficult to predict [1]. Therefore, studies have been performed to determine the factors that affect the tranquility of a harbor (e.g., [2]). For example, knowledge of short-period waves with wave periods less than 30 s, such as wind waves and swells, is an essential prerequisite for the planning and design of harbor protection structures [3], and numerical models have been employed to assess wave agitations induced by short waves in ports [4–6]. On the other hand, it has been suggested that long waves, including infragravity waves, might also be important factors that affect the harbor operation rate even when the harbor offers good protection against short waves [7–9], and low-frequency motions via harbor resonance could also cause agitations inside a harbor [10]. In addition, it was reported that the vertical movement of a vessel at berth was mainly determined by the swell energy inside the port basin, but the horizontal movement was strongly correlated with the low-frequency band energy [11].

In the case of Pohang New Port, it is difficult to determine the exact causes of the frequent downtimes, as its initial design changed due to port expansion, which meant that the combined effects of short waves, infragravity waves, and natural oscillation had to be considered. For example, it was suggested that the contribution of long waves and the

natural oscillation period could be also considerable [1]. On the contrary, there have been research results that support the concept that short gravity waves are still the major cause of the downtime in Pohang New Port [12–14], and a detached ~700 m long breakwater with 15 caissons was constructed from October 2018 to December 2020 according to these study results [15,16]. Therefore, the present study was designed to investigate the effectiveness of the detached breakwater in improving the harbor tranquility and thus to confirm the research results that suggested short waves are the main cause for the downtime in Pohang New Port. Previously, a similar experiment was conducted to analyze the effectiveness of a detached breakwater [17]. According to this study, the harbor tranquility was improved after a detached breakwater was constructed. However, the accuracy of the results was questioned [17] because the wave data outside the port were measured at the entrance of Yeongil Bay.

To resolve this problem, in the present study, we employed wave observation data measured at additional stations inside Yeongil Bay, both before and after the construction of the breakwater. The new wave data in this study were measured at three additional stations (W1, W6, and W7 in Figure 1). Therefore, one of the advantages of the present study is that the waves were measured (just) offshore of the detached breakwater, meaning that a direct comparison with the waves inside Pohang New Port increased the accuracy of the results. The most significant contribution of this study is that the harbor tranquility was closely investigated based on field wave data obtained from the observations in both periods before and after the construction of the detached breakwater. Therefore, we were able to examine the effect of the breakwater on the tranquility inside the port under various wave conditions that occurred in the real field. To the best of the authors' knowledge, most of the previous studies that investigated harbor tranquility were based on physical and numerical model experiments, laboratory experiments, or the application of artificial intelligence approaches. Field observation data were used in some previous studies, but only for limited times of the observational periods at daily scales. In this study, the results from the analysis of field data removed the uncertainties that could arise from the simulations that used models and AI approaches. The variety of the wave conditions during the experimental periods could also offer inferences for extreme cases through statistical data. In addition to the analysis of the observation data, a Boussinesq-type wave propagation model was used to conduct numerical experiments to support the observational results by investigating the mechanism during the courses of wave propagation before and after the construction of the breakwater.

The purpose of this study was to analyze the rate of the reduction of wave height inside Pohang New Port due to the construction of a detached breakwater by using improved wave observation data and also by using a phase-resolving wave model that is capable of simulating the effects of wave refraction and diffraction in the complicated topography near the port. In this study, we also aimed to investigate the effect of the breakwater by examining the reduction rate according to the wave propagation direction and thus to provide precedent data in designing future structures in similar environments.

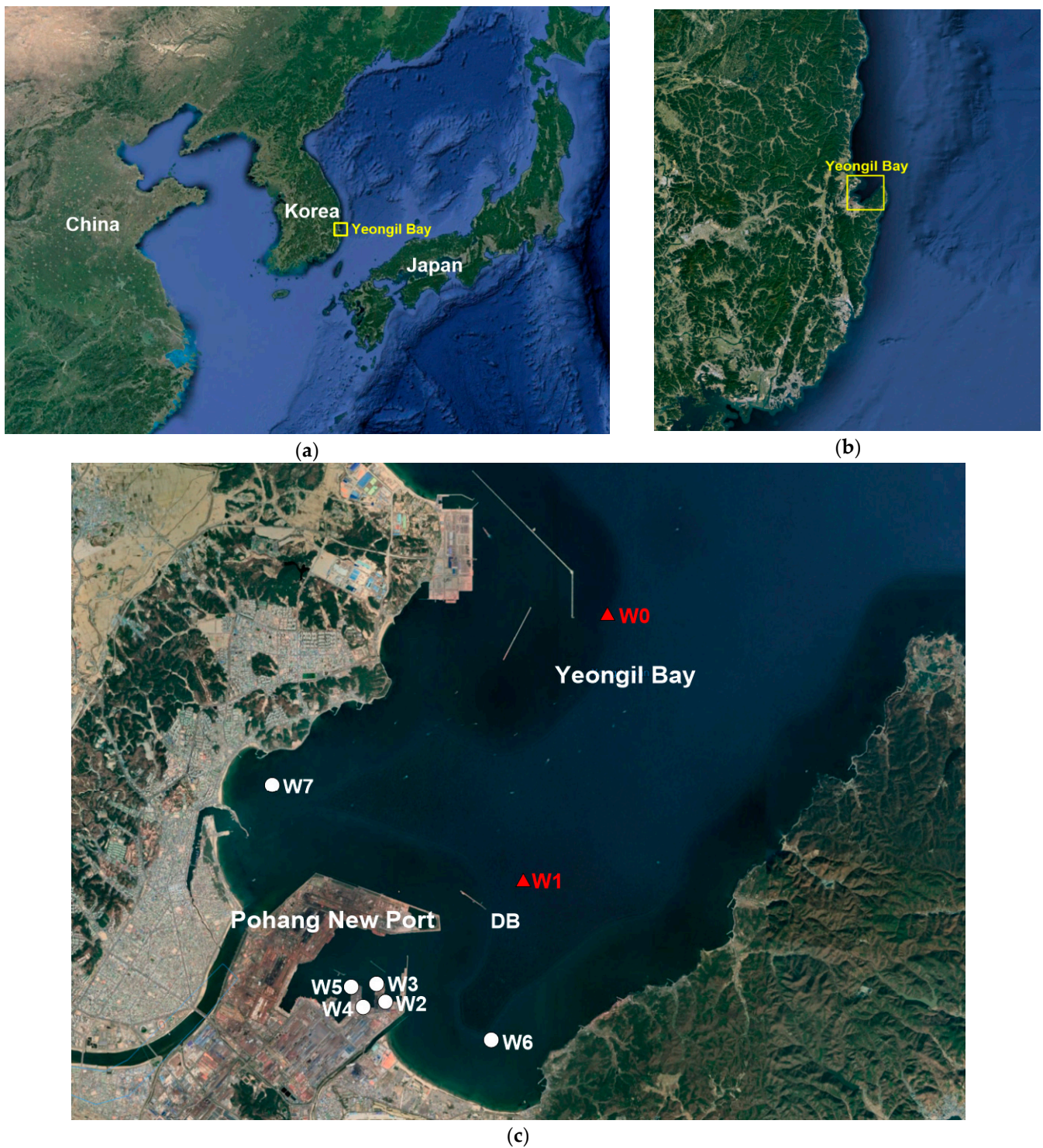


Figure 1. (a) Map of the Korean Peninsula with the location of Yeongil Bay, (b) map of Yeongil Bay located in the southeast of the Korean Peninsula, and (c) magnified map of Yeongil Bay with the locations of wave measurements. W0 and W1 (red triangles): locations where AWAC instruments were installed on the sea bed at the entrance of Yeongil Bay (W0) and just offshore of the detached breakwater (W1); W2–W5 (white circles): locations of the pressure sensors inside Pohang New Port; W6 and W7 (white circles): locations of pressure sensors in the nearshore of Dogu Beach (W6) and Yeongildae Beach (W7).

2. Materials and Methods

2.1. Study Site

Figure 1 shows the map of Yeongil Bay, captured from Google Earth, located in the southeast of the east coast of the Korean Peninsula, which is located in Northeast Asia. Yeongil Bay faces northeast with a mouth of ~10 km. Therefore, the waves that approach from the NE direction could reach the inner part of the bay and even affect the tranquility inside Pohang New Port [18]. As shown in Figure 1c, Pohang New Port was designed to protect the port from waves that mainly approach in the NE direction. However, the frequent downtime remained problematic in terms of the port's operation, which was unusual compared to the cases of other trading ports in the Republic of Korea.

As introduced in Section 1, previous research results have supported the concept that short gravity waves are the major cause for downtime in Pohang New Port, suggesting that harbor tranquility would be improved if the intrusion of short waves into the port was effectively prevented [12,14] and proposing that the target wave height to reach the desired harbor tranquility is 0.3 m [13]. As a measure to maintain the target wave height inside the port, it was suggested that a detached breakwater could be constructed outside the port to block approaching waves. Harbor breakwaters are usually constructed parallel to the shoreline near the edge of the surf zone to reduce the wave energy and protect the shore [19,20]. However, detached breakwaters have also been commonly constructed outside harbors to reduce the energy of waves that propagate to the harbor [21], along with other devices [22]. As a result, a detached, ~700 m long breakwater with 15 caissons was constructed from October 2018 to December 2020 [15,16]. In a previous study, the effect of the detached breakwater was investigated [17], and it was shown that the harbor tranquility was improved after the construction of the breakwater, as the frequency of the measured wave height exceeding the target wave height of 0.3 m clearly decreased. However, questions arose regarding the accuracy of the results of [17], because the wave data outside the port were measured at the entrance of Yeongil Bay. Due to the long distance from the wave station located at the bay entrance (W0 in Figure 1), the comparison with the wave data measured inside the port lowered the credibility of the analysis results. For example, the data in [17] showed that the breakwater was effective against waves in all directions measured at the bay entrance, W0. However, as shown in Figure 1, the course of wave propagation is varied inside Yeongil Bay, and waves from specific directions can successfully intrude into Pohang New Port, which implies that the effectiveness of the detached breakwater depends on the direction of the wave propagation.

2.2. Wave Measurement

Because Yeongil Bay is surrounded by land, the wave climate inside the bay is usually calmer than that outside the bay. However, waves could become harsh enough to cause severe coastline erosion in Yeongildae Beach when severe storm waves approach the site, even though the beach is located in the western corner of the bay [23]. Pohang New Port was constructed in 1985 at the southwest end of Yeongil Bay, as shown in Figure 1c, and the figure also shows the seven locations where waves were measured. An AWAC (Acoustic Wave And Current profiler) was installed on the sea bed at the entrance of Yeongil Bay (W0), as this is where waves were measured outside Pohang New Port in [17]. In this study, wave observations were carried out in W1, where an AWAC was installed on the sea bed ~1.2 km offshore from the head of the detached breakwater in the NE direction to measure the significant wave height (H_{m0}), peak wave period (T_p), and peak wave direction (D_p) every 30 min. Because an AWAC uses acoustic sensors to directly detect the wave surface elevation, it generally provides wave data with higher accuracy compared to a pressure transducer, which indirectly measures the surface elevation by converting the pressure time series using transfer functions [24]. During stormy conditions with strong wind, however, the white-capping of the waves disturbs the acoustic sensors, which may lower the accuracy of the AWAC measurements. In the case of W1, the AWAC was located inside the bay, and the wind energy was reduced as it was blocked by the land surrounding the

bay, securing the validity of the AWAC data during most of the observational periods. The AWAC was used to measure the wave data from 21 May 2018. Before then, a Directional Waverider buoy from Datawell Inc. was moored at the same location, W1, to observe the wave conditions for ~9 months from 15 October 2008 to 12 July 2009, and the data during this period were also used in this study. Inside Pohang New Port, pressure sensors and a WTG (Wave and Tide Gauge) were deployed to measure H_{m0} and T_p at the four stations (W2, W3, W4, and W5), and their data were available during the same time periods, with the data from W1 being used for comparison. In addition to these stations inside the port, wave data were also measured using a pressure sensor and a WTG in the nearshore of Dogu Beach (W6) located in the southeast corner of Yeongil bay ~1.4 km in front of the beach. Similarly, another WTG was deployed in the west corner of the bay (W7) ~1.0 km in front of Yeongildae Beach. Due to these wave measurements in W6 and W7, the changes in the wave environment before/after the detached breakwater construction could be observed over the wider area inside Yeongil Bay. The wave data in W6 and W7 were measured from 21 May 2018, and thus, were not available in 2008 and 2009. The locations of the wave sensors, measuring periods, and speculations of the instruments are listed in Table 1.

Table 1. List of observational instruments, locations, installation depths, and measuring frequency.

Station	Locations (Lat., Lon.)	Depth (m)	Instrument	Measuring Period	Measuring Frequency (Hz)
W0	36°05'21.90" N 129°28'21.20" E	D.L. (-)24.5	AWAC	21 May 2018–9 May 2020	2
W1	36°02'16.34" N 129°27'12.03" E	D.L. (-)22.0	Directional Waverider buoy	15 October 2008–12 July 2009	1.28
			AWAC	21 May 2018–9 May 2020	2
W2	36°00'46.30" N 129°25'05.60" E	D.L. (-) 8.5	WTG	15 October 2008–9 May 2020	2
W3	36°01'00.10" N 129°24'58.00" E	D.L. (-)11.0	WTG	15 October 2008–9 May 2020	2
W4	36°00'42.70" N 129°24'45.30" E	D.L. (-)10.0	WTG	15 October 2008–9 May 2020	2
W5	36°00'58.20" N 129°24'36.10" E	D.L. (-) 9.7	WTG	15 October 2008–9 May 2020	2
W6	36°00'21.15" N 129°26'39.83" E	D.L. (-)12.5	WTG	21 May 2018–9 May 2020	2
W7	36°03'22.65" N 129°23'25.86" E	D.L. (-) 8.5	WTG	21 May 2018–9 May 2020	2

As previously described, the effect of the detached breakwater was examined by separating the periods of wave measurements into two groups—before and after the construction of the breakwater. The 1st–6th caissons were placed between 15 October 2018 and 14 January 2019, and the 12th caisson was placed by 6 August 2019. In the present study, therefore, the period before construction (hereafter, BC) was set to the wave measurements that were conducted before 13 February 2019 when the 1st–6th caissons were placed (before the 7th caisson was placed), and the period after construction (hereafter, AC) was set to after 6 August 2019, when the 12th caisson was placed. The starting time of BC was set to 15 October 2008, when the observation in W1 started, and the ending time of AC was set to 9 May 2020. Therefore, two separate time periods were included in BC, as the first started from 15 October 2008 to 12 July 2009, during which the Directional Waverider buoy was installed in W1; this period lasted for 271 days. This first period of BC is abbreviated as BC01 hereafter. In BC01, the wave measurements were available at five (W1, W2, W3, W4, and W5) out of a total of eight stations. The second period in BC was from 21 May

2018 to 13 February 2019, which lasted for 269 days (hereafter, BC02). In BC02, the data in W2 were of poor quality, with a missing period of 85 days, which was excluded from the analysis. The AC period comprised 278 days from 8 August 2019 to 9 May 2020, and good-quality wave data were available at all measuring stations. The observational periods in BC (hereafter, BC refers the period that includes both BC01 and BC02) and AC are listed in Table 2.

Table 2. List of the observation periods.

	Period	Data Availability
Before construction (BC) of the detached breakwater	15 October 2008–12 July 2009 (271 days, BC01)	Avail.: 5 station N.A.: 3 stations (W0, W6, W7)
	21 May 2018–13 February 2019 (269 days, BC02)	Avail.: 7 station N.A.: 1 station (W2)
After construction (AC) of the detached breakwater	6 August 2019–9 May 2020 (278 days, AC)	Avail.: 8 station N.A.: 0 station

In Figure 2, H_{m0} , measured in W1 and W3, is plotted for both BC and AC to compare the wave height outside and inside Pohang New Port. The value of H_{m0} measured in BC01 is shown in Figure 2a, whereas the data measured in BC02 are shown in Figure 2b. The maximum H_{m0} measured in W1 was 3.4 m in BC on 26 April 2009 and 4.8 m in AC on 22 September 2019, showing that it was higher in AC by ~1.4 m. In BC, there were ~168 h in which there were high wave conditions in which H_{m0} in W1 was greater than 2 m, and in AC, there were ~332 h. Considering that the BC period was longer (540 days) than the AC period (278 days), it was found that the wave conditions were more energetic during AC. In contrast, the maximum H_{m0} measured in W3 was 0.98 m in BC on 26 April 2009 and 0.64 m in AC on 22 September 2019, showing that it was higher in BC by ~0.34 m. In addition, in BC, there were ~183 h in which H_{m0} was higher than 0.5 m in W3, and this was a much shorter time in AC, as it was ~10 h. Considering that the wave condition was generally higher in AC outside the port, the shorter period in which H_{m0} was greater than 0.5 m in AC indicates that the detached breakwater clearly reduced the wave height inside the port. In Figure 2, the waves measured in W1 were used as the data outside the port instead of those measured in W0, and the reason for this is described in Section 3.

2.3. Selection of Wave Events

In order to examine the effect of the detached breakwater more closely, wave events were selected to filter out the calm wave conditions in which the breakwater effect could not be clearly observed because the wave energy was low both outside and inside the port. The wave events were selected by considering two conditions. The first was that H_{m0} should be higher than 1 m in W1. The second condition was that the time in which H_{m0} was greater than 1 m should last for at least 12 h so as to exclude inconsistent data. The number of selected wave events was 38 in BC and 27 in AC, the total time that corresponded to these wave events was 1150 h in BC and 1091 h in AC, and the time required for statistics was secured sufficiently. In Figure 3, time variations in wave height in W1 and W3 and wave direction in W1 are compared between the wave event examples selected in BC and AC. In both cases, the example events were selected as they had the maximum wave heights during each period. Therefore, for BC, a period of two days from 26 April 2009 was chosen as the example event. During this period, the H_{m0} value in W1 increased to a maximum of ~3.4 m, and the H_{m0} value in W3 increased to ~1.0 m. The wave direction range was N15°E~N50°E, showing that the waves generally approached in the NNE and NE directions, as these are the primary wave propagation directions in this region. For AC, a period of four days from 21 September 2019 was chosen as the example event; the H_{m0} value in W1 increased to its maximum value of ~4.8 m, and the H_{m0} value in W3 increased

to ~0.6 m. The wave direction range was N40°E~N60°E, showing that the waves generally approached in the NE direction during this storm period.

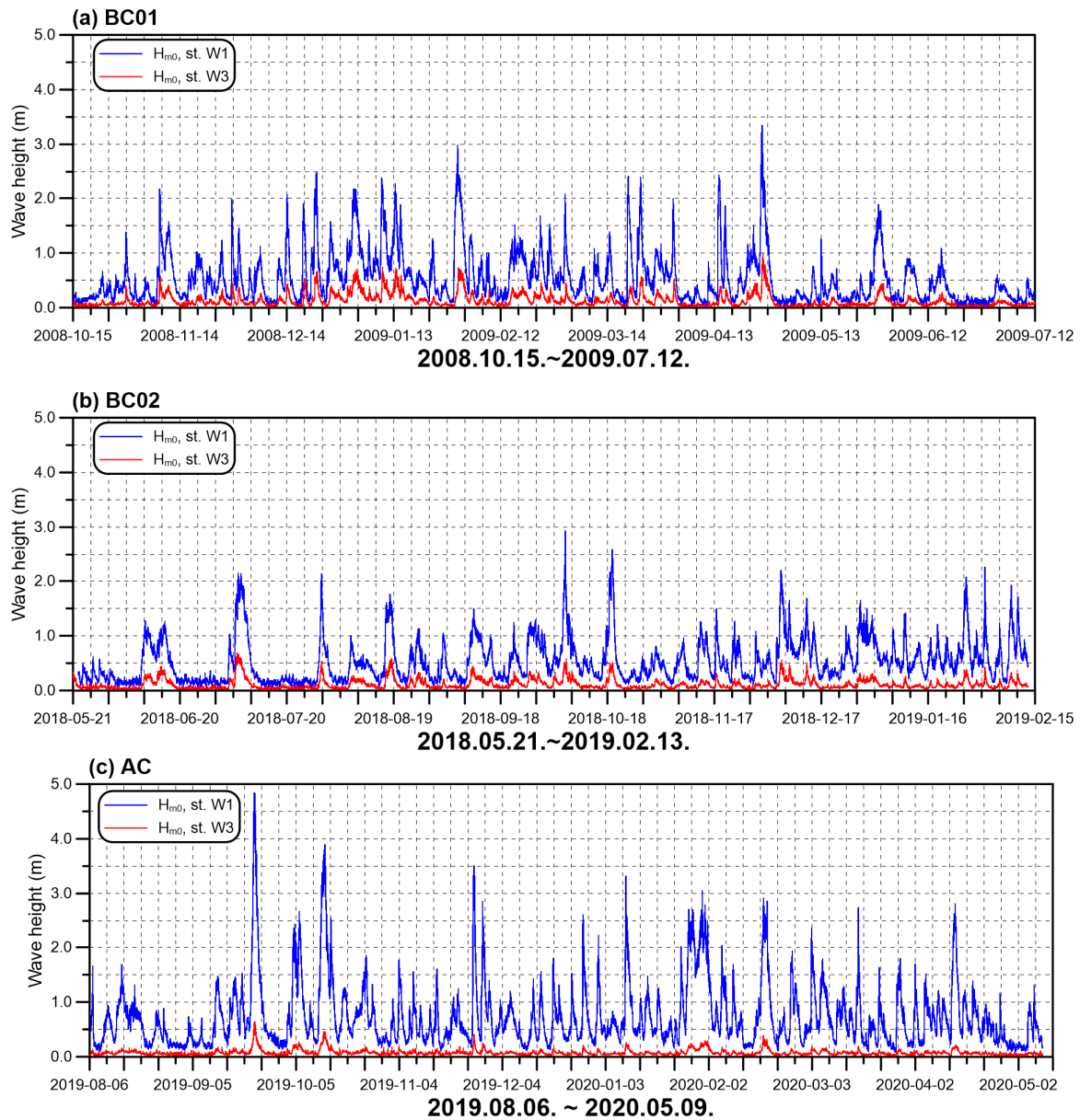


Figure 2. Comparison of H_{m0} in W1 (blue) and W3 (red): (a) first period before detached breakwater construction (BC01) in 15 October 2008–12 July 2009, (b) before detached breakwater construction (BC02) in 21 May 2018–13 February 2009, and (c) after detached breakwater construction (AC).

2.4. Numerical Model Experiment

The BOUSS-2D wave model was employed to conduct numerical experiments to understand the results from the observational data. The observation results showed the breakwater reduced the wave energy inside the port through a comparison of wave height measurements between BC and AC. However, this comparison could not provide the detailed ways in which the reductions actually occurred, which would require additional numerical experiments to understand the processes of wave transformation. The BOUSS-2D wave model was developed based on the non-linear Boussinesq equations [25], and the background of the model is described as follows. The classical form of the Boussinesq equations for wave propagation over water of variable depth was derived by [26], and

the equations were restricted to relatively shallow water depths ($h < L/5$ with $h =$ water depth and $L =$ wave length). Nwogu [27] extended the range of applicability of the Boussinesq-type equations to deeper water. Despite this improvement, these equations were based on the assumption that wave heights are much smaller than the water depth. This limited the ability of the equations to describe highly non-linear waves in shallow water and led to a fully non-linear form of equations that are useful for the simulation of asymmetric waves in shallow water, wave-induced currents, wave setup, and wave-current interaction [28]. Then, Nwogu [29] extended the fully non-linear form of Boussinesq equations to the surf zone to consider the turbulence generated by breaking waves and the effect of bottom friction. These modified equations were able to simulate most of the hydrodynamic phenomena in the coastal regions and harbor basins, which included shoaling, refraction, diffraction, reflection, bottom friction, wave-wave and wave-current interactions, wave-induced currents, and wave breaking and runup. The BOUSS-2D model has been successfully applied to simulate wave diffraction in the lee of coastal structures and wave propagation over relatively steep slopes.

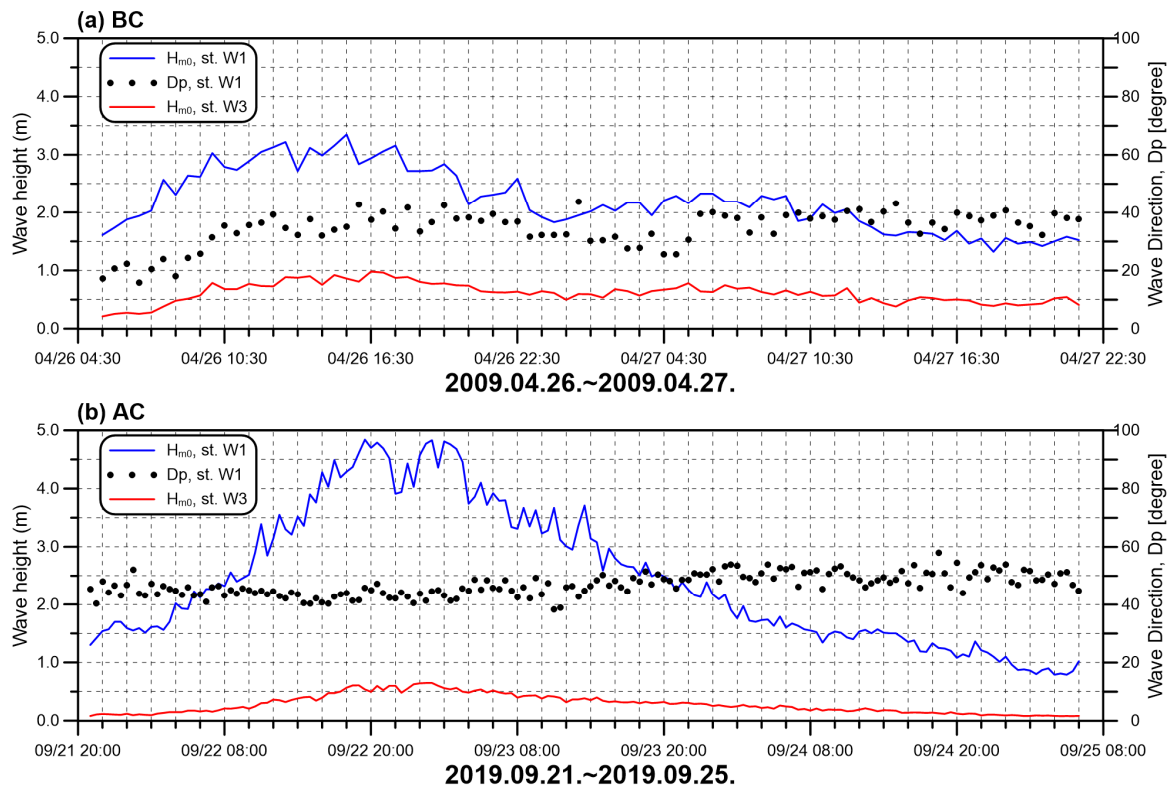


Figure 3. (a) H_{m0} (blue line) and D_p (black circles) in W1 and H_{m0} in W3 (red line) for a selected wave event in BC; (b) same as (a) but an event in AC. These two wave events were also selected for the numerical experiments, as described in Sections 2.3 and 3.2.

BOUSS-2D equations are depth-integrated equations for the conservation of mass and momentum for non-linear waves propagating in shallow and intermediate water depths. They can be considered to be perturbations from shallow-water equations, which are often used to simulate tidal flows in coastal regions. For short-period waves, the horizontal velocities are no longer uniform over depth, and the pressure is non-hydrostatic. The vertical profile of the flow field is obtained by expanding the velocity potential, Φ , as a Taylor series for an arbitrary elevation, z_α , in the water column. For waves with length, L , much longer than the water depth, h , the series is truncated at the second order, resulting in a quadratic variation in the velocity potential over depth:

$$\Phi(x, z, t) = \phi_\alpha + \mu^2(z_\alpha - z)[\nabla\phi_\alpha \cdot \nabla h] + \frac{\mu^2}{2} [(z_\alpha + h)^2 - (z + h)^2] \nabla^2\phi_\alpha + O(\mu^4) \quad (1)$$

where $\phi_\alpha = \Phi(x, z_\alpha, t)$, $\nabla = (\partial/\partial x, \partial/\partial y)$, and $\mu = h/L$ is a measure of frequency dispersion. The horizontal and vertical velocities are obtained from the velocity potential as:

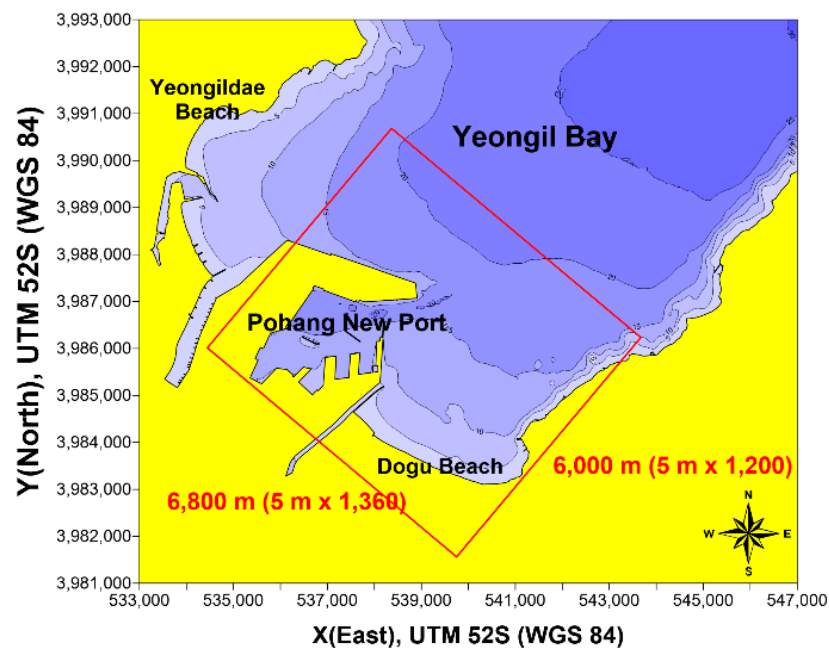
$$u(x, z, t) = \nabla\Phi = u_\alpha + (z_\alpha - z)[\nabla(u_\alpha \cdot \nabla h) + (\nabla \cdot u_\alpha)\nabla h] + \frac{1}{2} [(z_\alpha + h)^2 - (z + h)^2] \nabla(\nabla \cdot u_\alpha) \quad (2)$$

$$w(x, z, t) = \frac{\partial\Phi}{\partial z} = -[u_\alpha \cdot \nabla h + (z + h)\nabla \cdot u_\alpha] \quad (3)$$

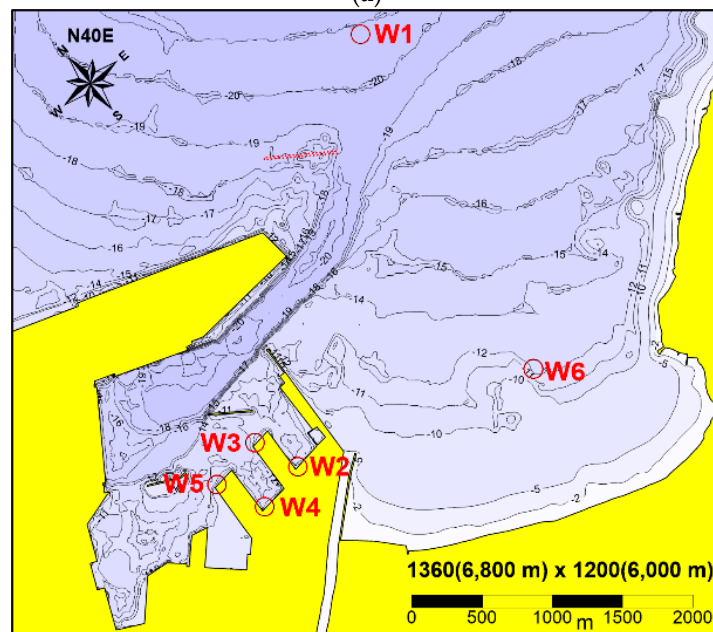
where $u_\alpha = \nabla\Phi|_{z_\alpha}$ is the horizontal velocity at $z = z_\alpha$. Given a vertical profile for the flow field, the continuity and Euler (momentum) equations can be integrated over depth, reducing the three-dimensional problem to two dimensions. For more detailed information regarding the BOUSS-2D model, readers are referred to the manual in [25].

In this study, the BOUSS-2D model was set up in a rectangular grid system using the staggered method by calculating the time-varying surface elevation and horizontal velocities at the grid nodes. The computational domain around Pohang New Port is shown in Figure 4. A rectangular domain with a size of 6.8 km by 6.0 km was set up by rotating the domain to the NE direction so that the outer open boundary could face N40°E (Figure 4a). This was because the majority of the waves approach in the NNE and NE directions in this region, and the input wave directions forced along the open boundary could range within $\pm 30^\circ$, which is important for the stability of the model runs. The Δx and Δy of each grid was 5 m and set uniformly in the whole domain; thus, a total of 1360 grid points were allotted in the x-direction (parallel to detached breakwater), and 1200 grids were allotted in the y-direction.

The model was run for two different cases, representing the wave conditions in BC and AC, respectively. The two cases were the same as the selected events shown in Figure 3. That is, the model was run from 05:30 on the 26 to 21:30 on the 27 April 2009 for BC and from 07:00 on the 22 to 21:00 on the 23 September 2019 for AC. The BOUSS-2D model is not stable when used with waves of periods shorter than 8 s, meaning that the two cases were run for the times during which the observed periods were longer than 8 s. As it was not practical to continuously run BOUSS-2D for the whole time of 38–40 h, which had varying wave conditions, as shown in Figure 3, the experiment was conducted by running the model at every hour by specifying the directional spectra that represented the wave conditions at the corresponding time. In the case of BC, for example, the model was run 39 times, corresponding to each hour from 05:30 on the 26 to 21:30 on the 27 April 2009, with the model being forced to be determined from the data measured at each hour. Individual runs were simulated for 3900–4000 s until a stable condition was reached with $\Delta t = 0.15$ s. These numerical experiments were designed to understand the course of wave energy reduction between BC and AC through model validation via comparisons with observational data. The results are discussed in Sections 3.2 and 4.



(a)



(b)

Figure 4. (a) Map of Yeongil Bay around Pohang New Port, in which the computational domain for the BOUSS-2D wave model is marked in a red rectangle, (b) model domain with the bathymetry map and the locations of wave stations. It is noted that the domain is rotated 40° in the NE direction for the outer open boundary to face N40°E.

3. Results

3.1. Observational Data

The number of wave events that consistently had wave heights greater than 1 m for at least 12 h was 38 in BC and 27 in AC, as described in Section 2. The selected events generally corresponded to the times when high waves, including storms, were present in Yeongil Bay, and H_{m0} displayed increasing and decreasing patterns during these periods, as shown in Figure 3. Therefore, there was a time when the H_{m0} value became the maximum, and the H_{m0} value at this time was selected as the representative value for each event. In Figure 5, the maximum H_{m0} values of all of the events are compared between W1 (outside

Pohang New Port) and W2, W3, W4, and W5 (inside Pohang New Port) in BC and AC. Similarly, the representative values for the wave propagation direction, D_p , were selected at the same time at which the maximum H_{m0} values for the corresponding events were observed. In Figure 6, the representative D_p value measured in W1 is compared with the H_{m0} value in W2, W3, W4, and W5.

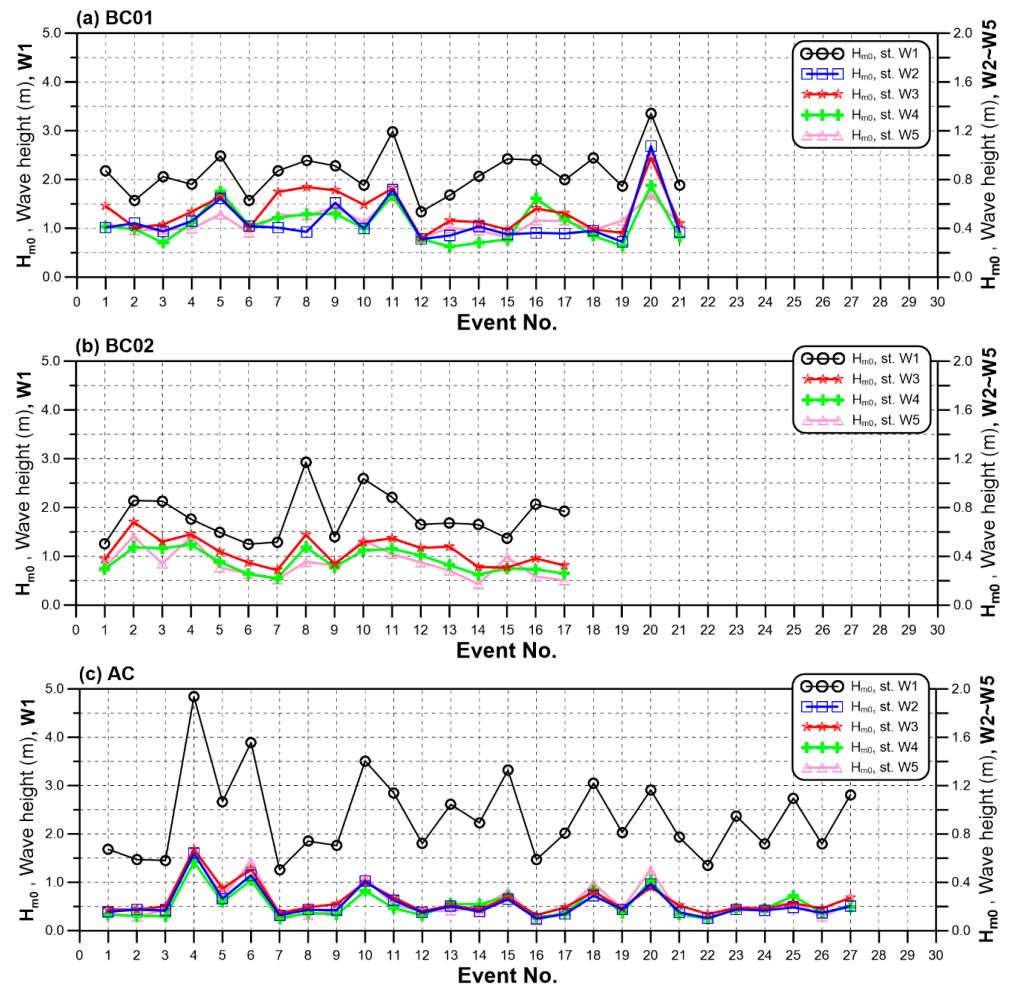


Figure 5. (a) Maximum values of H_{m0} observed in the 21 events before construction in W1 (black circles), W2 (blue squares), W3 (red stars), W4 (green crosses), and W5 (pink triangles) for BC01 (15 October 2008~12 July 2009); (b) maximum H_{m0} values for the 17 events before construction in W1 (black circles), W3 (red stars), W4 (green crosses), and W5 (pink triangles) for BC02 (21 May 2018~13 February 2019) (it is noted that the H_{m0} in W2 was not included due to poor data quality); (c) maximum H_{m0} values for the 27 events after the construction in W1 (black circles), W2 (blue squares), W3 (red stars), W4 (green crosses), and W5 (pink triangles). The pattern of H_{m0} variation is similar between the wave stations outside (W1) and inside (W2, W3, W4, and W5) the port.

In the case of wave height, the H_{m0} varied with the wave events and showed similar patterns at all stations, as when the H_{m0} value was high inside the port (W2, W3, W4, and W5), the H_{m0} value was generally also high outside the port (W1). It is noted that the representative H_{m0} values inside the port were mostly higher than 0.2 m, and ~50% of them were even higher than 0.4 m in BC. In contrast, in AC, the representative H_{m0} values outside the port in 23 events out of a total of 27 events were lower than 0.4 m, and ~50% of them were even lower than 0.2 m, which indicates that the breakwater effectively reduced the wave energy inside the port. In the case of the representative D_p value, its correlation with the representative H_{m0} was lower, as shown in Figure 6. In the second period of BC (Figure 6b), the representative D_p value in W1 showed a large discrepancy with the H_{m0}

measured inside the port. The D_p measured in W1 was greater than 40° in events #1–#7, whereas the D_p value became lower than 25° in events #8–#17. However, this pattern was not observed in terms of the H_{m0} value inside the port. In AC, a similar conclusion was not easily found, because there were wave events such as #4, #6, #10, and #20 when the H_{m0} value in W2, W3, W4, and W5 increased and the D_p value in W1 was also greater than 30° ; thus, a correlation was observed between the wave direction and the height inside Pohang New Port.

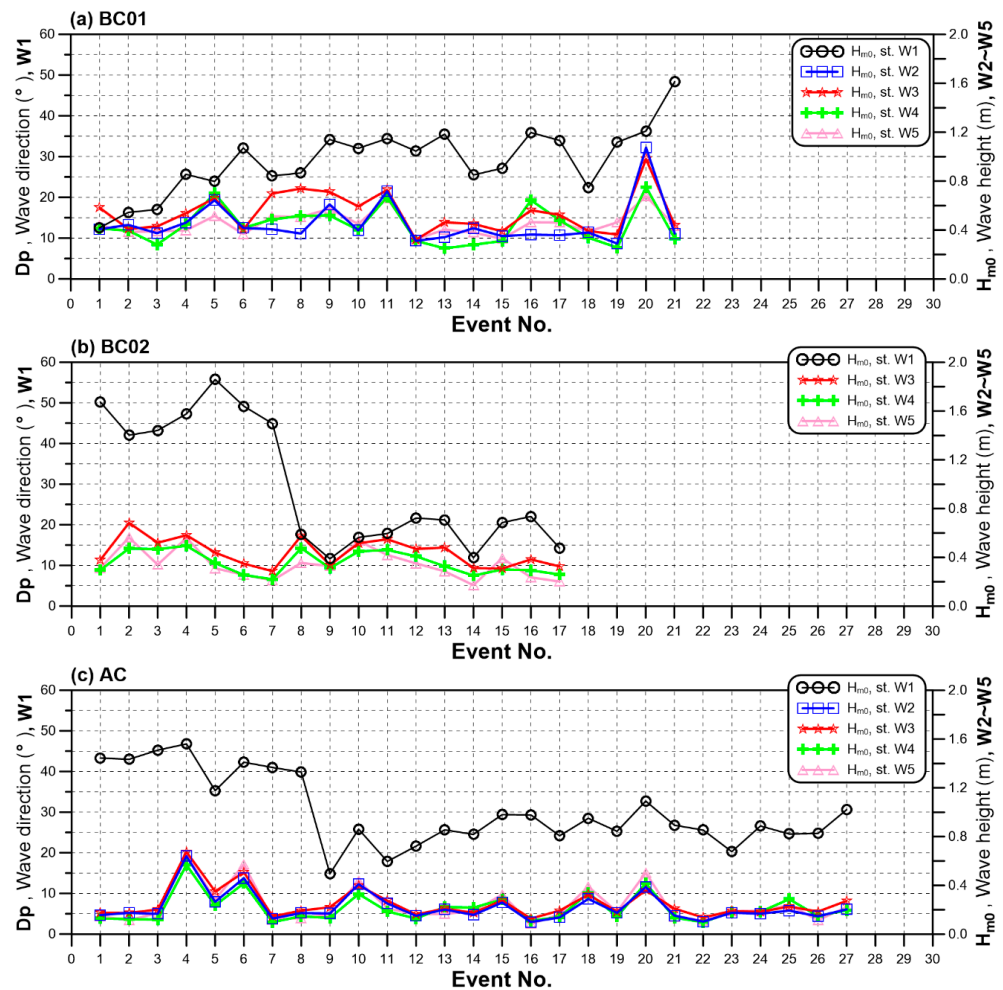


Figure 6. Same as Figure 5 but for D_p values that were observed at the same time as the H_{m0} in Figure 5 (i.e., D_p in Figure 6 was measured at the time when the H_{m0} value was maximum for each wave event). Compared to the results in Figure 5, it shows a lower correlation between D_p outside the port (W1) and H_{m0} inside the port (W2, W3, W3, and W4).

In Figure 7, H_{m0} and D_p are compared between the measurements at the two stations, W0 and W1. It is noted that the waves were not measured in W0 during BC01 (2008–2009), meaning that Figure 7 only compares the data at BC02 (2018–2019) and AC. In the case of H_{m0} , the data between the two locations show relatively high correlation with an r^2 , the coefficient of determination, of 0.84. However, the r^2 for D_p was as low as 0.16 between W0 and W1, which indicates that the directions of the waves that approached Yeongil Bay were not correlated with those that approached the detached breakwater. Therefore, to carry out a detailed investigation, it was necessary to examine the impact of wave direction based on the data in W1, as proposed in Section 1, in addition to the analysis based on the data in W0, which was conducted in [17]. In the present study, therefore, the data in W1 were considered the primary wave measurements outside Pohang New Port.

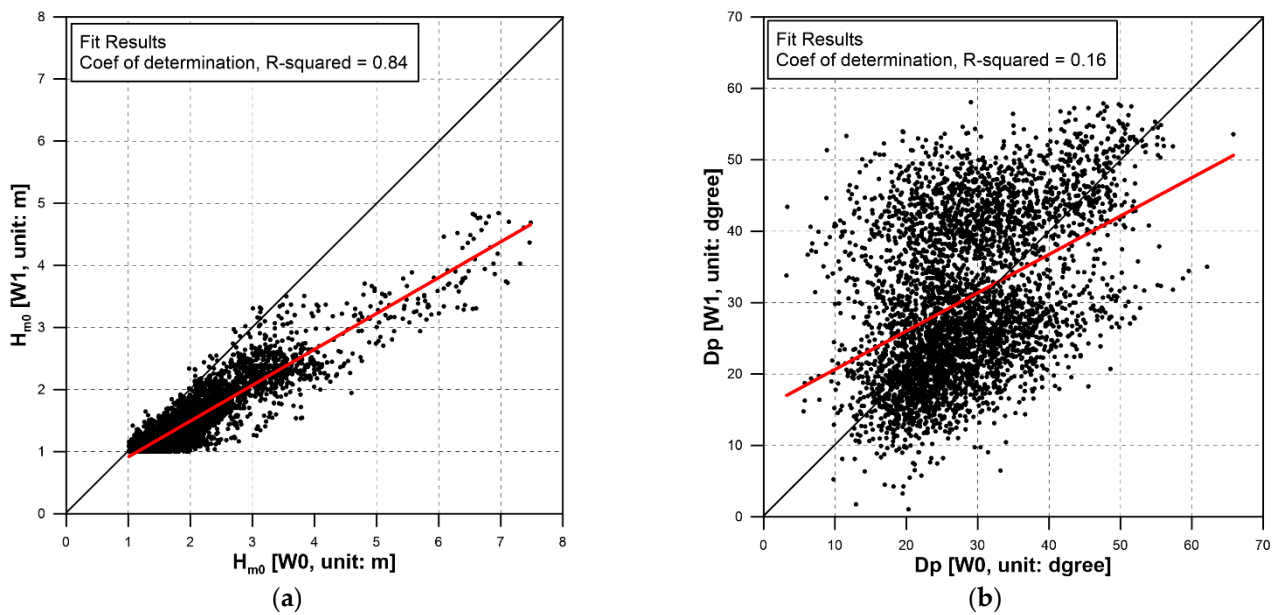


Figure 7. Comparison of the distributions of (a) significant wave height (H_{m0}) and (b) peak wave direction (D_p) between W0 and W1 for the selected events for both BC (only for the second period from 2018 to 2019) and AC. The coefficient of determination (r^2) was 0.83 for H_{m0} and 0.16 for D_p . Wave measurements show a high correlation in H_{m0} between the two wave stations of W0 and W1, whereas they show a lower correlation in the case of D_p .

The correlation between the wave parameters inside and outside Pohang New Port was examined by defining a new parameter, the wave height reduction rate ($R_{W\#}$). $R_{W\#}$ was calculated from the ratio of H_{m0} measured inside and outside the port (i.e., $R_{W2} = H_{m0}[W2]/H_{m0}[W1]$ and $R_{W3} = H_{m0}[W3]/H_{m0}[W1]$, etc.). The $R_{W\#}$ parameters were estimated from the data sets of 38 and 27 wave events selected for BC and AC, respectively, as described in Section 2.2, because the relationship between $R_{W\#}$ and D_p was not clearly observed for waves with low energy. In Figures 8 and 9, the distributions of $R_{W\#}$ versus D_p in W1 for the data selected for the wave events are compared between BC and AC. In addition to the four stations inside the port, the R_{W6} and R_{W7} values were estimated outside the port as well. Considering that the wave energy inside the port decreased with the decreasing magnitude of $R_{W\#}$, the results in Figures 8 and 9 clearly show that the wave energy was much reduced in AC compared to that in BC, confirming the effectiveness of the detached breakwater in reducing the wave energy inside the port. It is also interesting to see that the $R_{W\#}$ value measured inside the port ($R_{W2} - R_{W5}$) tended to increase with D_p , showing that the $R_{W\#}$ value increased as the wave direction in W1 changed from N to NE. In contrast, the opposite phenomenon occurred in W6, the station in front of Dogu Beach outside the port (Figure 1c), at which the R_{W6} value decreased with increasing D_p . On the other hand, the pattern in W7, the station in front of Yeongildae Beach, became similar to that inside the port, as the R_{W7} value also increased with increasing D_p . The difference in the pattern of $R_{W\#}$ with D_p in W6 and W7 might have been induced by their locations, which is discussed in Section 4. The correlation between $R_{W\#}$ and D_p in BC was repeated in AC. However, the magnitude of $R_{W\#}$ measured inside the port was much lower in AC than that in BC, as its values in AC were ~50% of those in BC, which is discussed in Section 4. In Figures 8 and 9, the red lines show linear regressions and the regression coefficients are listed in Table 3.

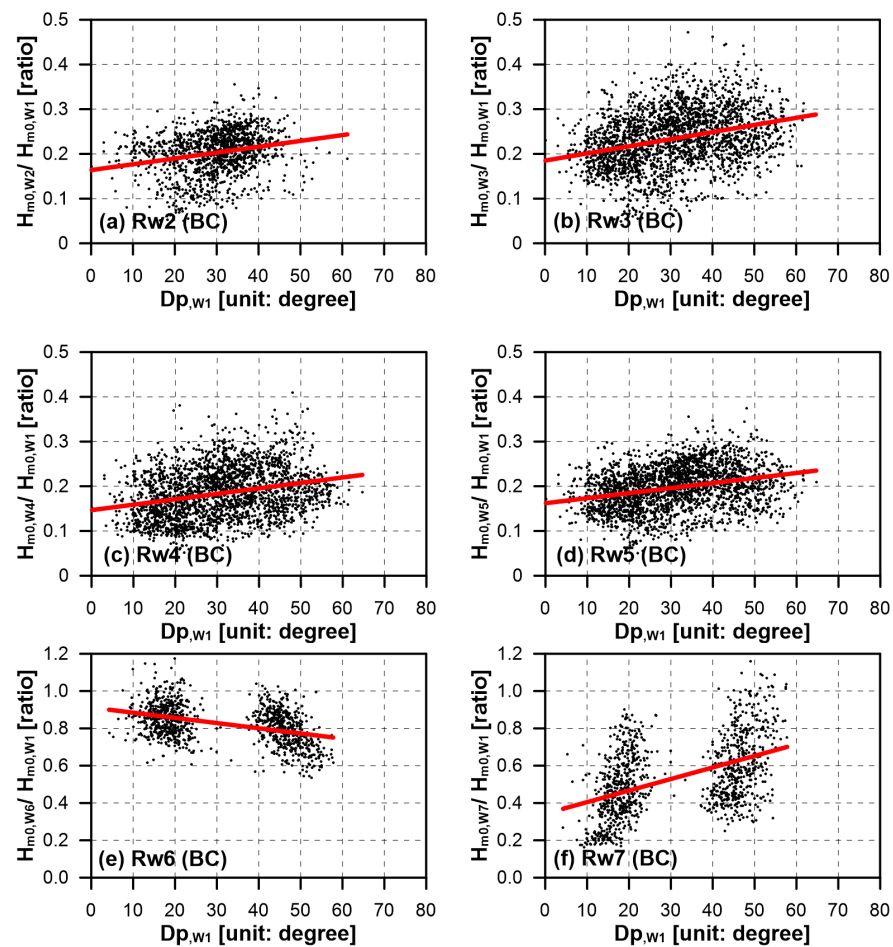


Figure 8. Scattered plots of $R_{W\#}$ [$R_{W2} (= \frac{H_{m0}[W2]}{H_{m0}[W1]}), R_{W3} (= \frac{H_{m0}[W3]}{H_{m0}[W1]}), R_{W4} (= \frac{H_{m0}[W4]}{H_{m0}[W1]}), R_{W5} (= \frac{H_{m0}[W5]}{H_{m0}[W1]})$] versus D_p measured in W1 for the data measured during the 38 wave events in BC. (a) R_{W2} vs. D_p , (b) R_{W3} vs. D_p , (c) R_{W4} vs. D_p , (d) R_{W5} vs. D_p , (e) R_{W6} vs. D_p , (f) R_{W7} vs. D_p . The red line in each panel shows the linear regression calculated for each data set. It is noted that R_{W2} was calculated from the BC01 data (2008–2009) due to the poor quality of the measurements in BC02 (2018–2019). In addition, BC01 data were not available in the case of R_{W6} and R_{W7} , as the waves were not measured in these stations in the 2008–2009 experimental period. $R_{W\#}$ consistently tended to increase with increasing $D_p, W1$ in the wave stations inside the port (W2, W3, W4, and W5) and that located in the west corner of Yeongil Bay (W7), whereas $R_{W\#}$ decreased with increasing $D_p, W1$ in the wave station located in the southeast corner of the bay.

Considering that the D_p value measured in W1 acted as a controlling factor on the wave reduction inside Pohang New Port, it was also necessary to examine the impact of the wave height on the wave reduction pattern. Figures 10 and 11 show the scatter plots between $R_{W\#}$ and H_{m0} , measured in W1. It is observed that $R_{W\#}$ did not show a clear correlation with H_{m0} in W1 for both BC and AC. It is noted that the time variation pattern of H_{m0} measured inside the port was similar to that of H_{m0} in W1, as shown in Figures 2 and 5. Therefore, the low correlation between $R_{W\#}$ and H_{m0} inside the port was an interesting result, indicating that the wave reduction process inside the port might not be dependent on the wave height, unlike the wave direction. The low correlation between $R_{W\#}$ and H_{m0} was not only observed inside the port but also outside the port in W6 and W7 in both BC and AC. The results in this section are important, because the effect of the breakwater was confirmed, as not only the magnitude but also the variance in $R_{W\#}$ were significantly reduced in AC compared to those in BC, regardless of the wave height. In addition, the high dependence of the wave reduction process inside the port on the propagation direction of short waves outside the port required further analysis to understand the courses of wave propagation around the breakwater and the port, which

was carried out using the BOUSS-2D model, which can simulate wave transformation around these complex structures, and the results are provided in the next section.

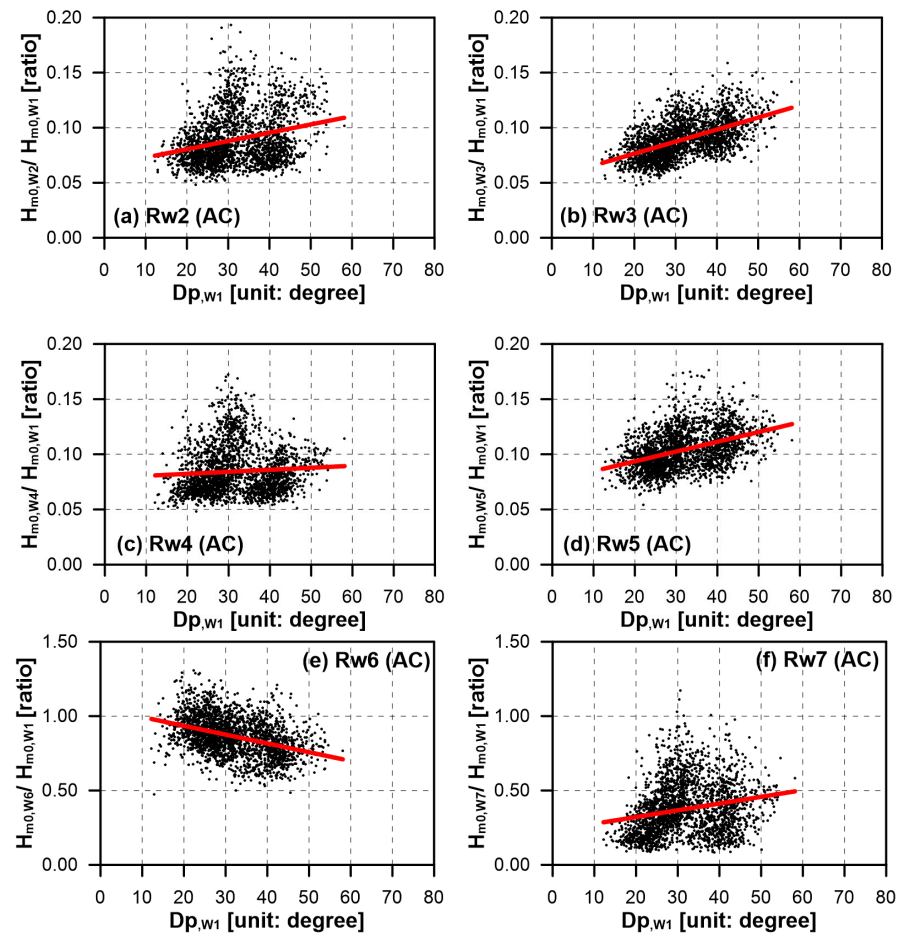


Figure 9. Same as Figure 8, but for the data measured during the 27 wave events in AC. Similar to the case of BC, it was found that $R_{W\#}$ consistently tended to increase with increasing $D_{p,W1}$ in the wave stations inside the port (W2, W3, W4, and W5) and that located in the west corner of Yeongil Bay (W7), whereas $R_{W\#}$ decreased with increasing $D_{p,W1}$ in the wave station located in the southeast corner of the bay.

Table 3. List of coefficients of determination (r^2) and linear regression coefficients (slope and intercept) for the scatter plots in Figures 8–11.

Figure 8	(a)	(b)	(c)	(d)	(e)	(f)
r^2	0.055	0.097	0.072	0.084	0.172	0.225
Linear regression	$0.0013X + 0.1638$	$0.0016X + 0.1850$	$0.0012X + 0.1468$	$0.0011X + 0.1621$	$-0.0028X + 0.9121$	$0.0062X + 0.3428$
Figure 9	(a)	(b)	(c)	(d)	(e)	(f)
r^2	0.072	0.296	0.005	0.168	0.149	0.047
Linear regression	$0.0008X + 0.0654$	$0.0011X + 0.0546$	$0.0002X + 0.0787$	$0.0009X + 0.0760$	$-0.0059X + 1.0529$	$0.0045X + 0.2308$
Figure 10	(a)	(b)	(c)	(d)	(e)	(f)
r^2	0.035	0.000	0.000	0.014	0.011	0.000
Linear regression	$-0.0212X + 0.2364$	$-0.0031X + 0.2388$	$-1.2018X + 0.1810$	$-0.0142X + 0.2184$	$0.0299X + 0.7804$	$0.0053X + 0.5318$
Figure 11	(a)	(b)	(c)	(d)	(e)	(f)
r^2	0.104	0.032	0.016	0.011	0.002	0.034
Linear regression	$0.0115X + 0.0690$	$0.0045X + 0.0813$	$0.0041X + 0.0772$	$0.0029X + 0.0991$	$0.0091X + 0.8489$	$0.0640X + 0.4936$

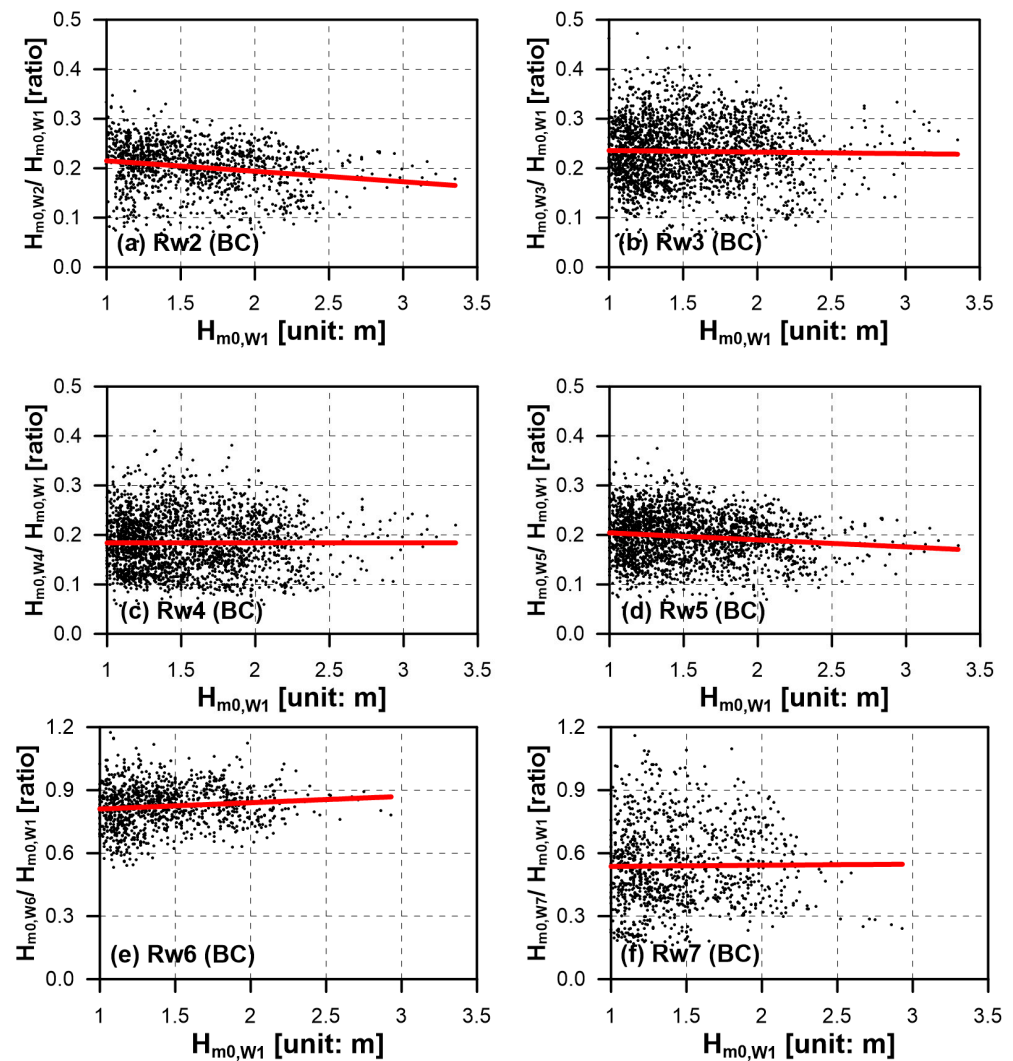


Figure 10. Same as Figure 8, but the x-axis is H_{m0} measured in W1 in BC. (a) R_{W2} vs. H_{m0} , (b) R_{W3} vs. H_{m0} , (c) R_{W4} vs. H_{m0} , (d) R_{W5} vs. H_{m0} , (e) R_{W6} vs. H_{m0} , (f) R_{W7} vs. H_{m0} . The correlation between $R_{W\#}$ and the wave propagation direction ($D_{p,W1}$) observed in Figures 8 and 9 was not found in the case of the wave height (H_{m0}).

3.2. Numerical Model Results

The BOUSS-2D wave model was set up as described in Section 2.3 for the two cases representing the wave propagation in BC and AC. The two cases were selected because they had the maximum wave heights during the period of the 38 (BC) and 27 (AC) wave events, as shown in Figure 3a,b. The events with the maximum H_{m0} were selected because the effect of the detached breakwater in reducing the wave energy inside Pohang New Port could be more clearly observed under higher wave energy conditions.

In Figure 12, the wave conditions in W1 are compared between the observed and modeled data from 26 to 27 April 2009, which were selected from the BC events. Considering the computational domain shown in Figure 4b, the location of W1 was close to the outside open boundary, and the modeled wave conditions were well matched with the observation data that were used for the boundary forcing conditions. The data show that the wave height increased to the maximum ($H_{m0} \sim 3.4$ m) at 15:30 on 26 April 2009, and then, it gradually decreased. The wave period fluctuated between 9.2 and 12.2 s, and the D_p value gradually increased from $\sim N12^\circ E$ to $\sim N40^\circ E$, indicating that the waves were mainly approaching from NNE~NE in W1 during this wave event.

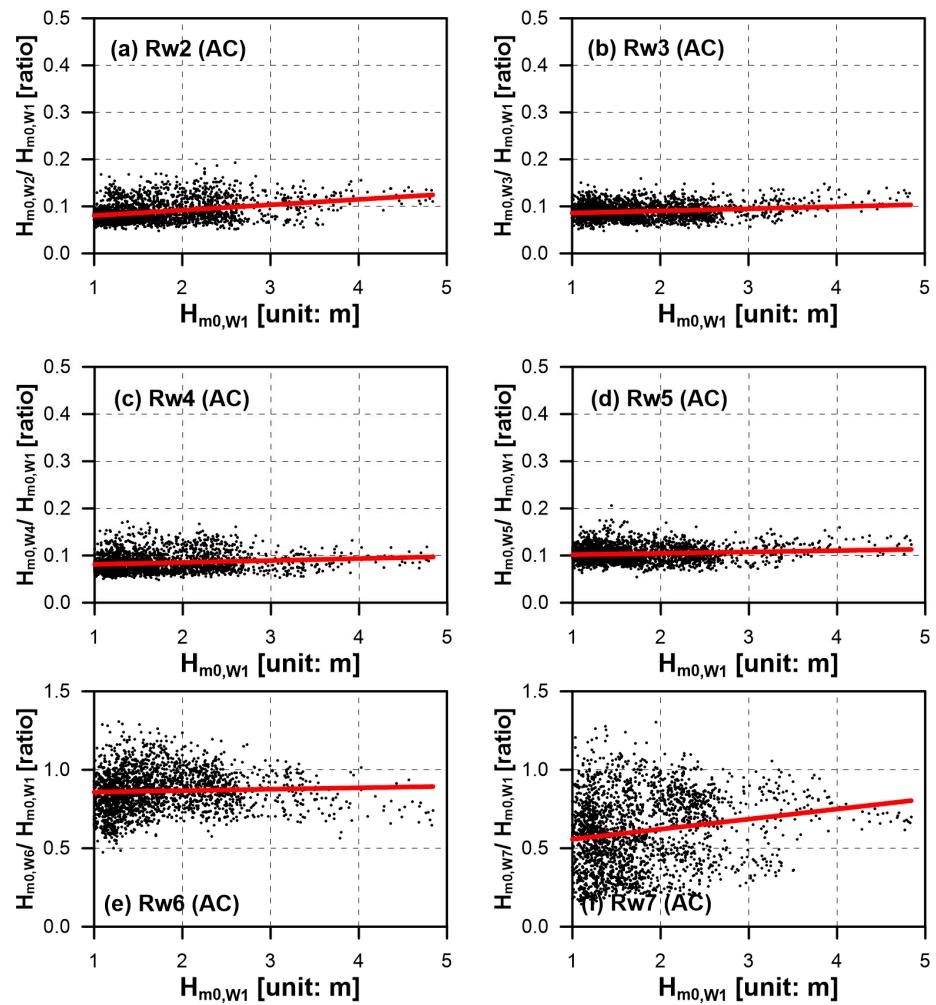


Figure 11. Same as Figure 10, but in AC. (a) R_{W2} vs. H_{m0} , (b) R_{W3} vs. H_{m0} , (c) R_{W4} vs. H_{m0} , (d) R_{W5} vs. H_{m0} , (e) R_{W6} vs. H_{m0} , (f) R_{W7} vs. H_{m0} . The correlation between $R_{W\#}$ and the wave propagation direction ($D_{p,W1}$) observed in Figures 8 and 9 was not found in the case of the wave height (H_{m0}).

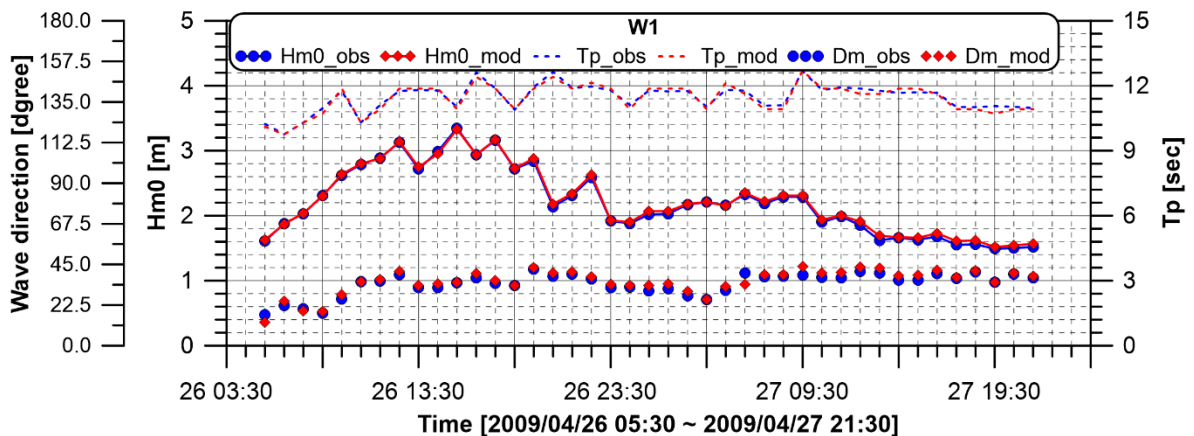


Figure 12. Comparison of wave conditions (H_{m0} , T_p , and D_p) between the observational (blue) and modeled (red) data in W1 during the period of the wave event selected for BC from 05:30 on the 26th to 21:30 on 27 April 2009 (39 h). It is noted that the modeled data matched well with the observational data due to the proximity of W1 to the open boundary, as shown in the computational domain (Figure 4b).

Figure 13 shows the comparisons of the modeled wave heights with observations at the four wave stations (W2, W3, W4, and W5) inside Pohang New Port to validate the model performance. Reasonable agreement was observed among the four wave stations inside the port (marked in Figure 4b), as the overall pattern of the H_{m0} time variation generally agreed between the modeled and observation data, although the model results were underestimated, specifically in W3 and W5. The average error ($\frac{\sqrt{(H_{obs}-H_{mod})^2}}{H_{obs}} \times 100$) was calculated, and it ranged from 12% to 23% (12.9%, 18.7%, 13.6%, and 22.7% for W2, W3, W4, and W5, respectively). It is noted that the errors were greater in the stations located outside the slits (W3 and W5) than those located inside the slits (W2 and W4). Although the reason for this is not yet clearly understood, the four wave stations were located in the corners of the slits where the incoming and reflected waves were interfered with in complicated ways, which could have increased the wave height compared to that in other areas near the slits and also could have increased the modeling errors. As the pattern of the H_{m0} time variation of the model generally agreed with that shown in the observation, it could be concluded that the model was validated for the wave event, and the model results were further analyzed to understand the wave propagation pattern inside the port.

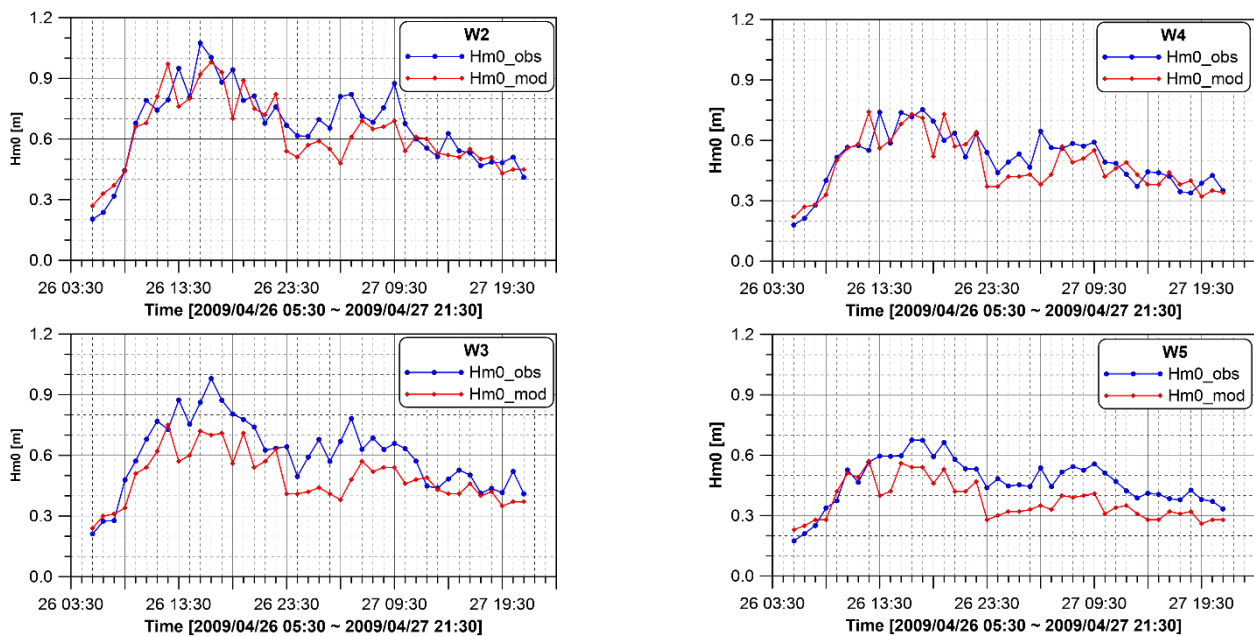


Figure 13. Comparison of wave height (H_{m0}) between the observational (blue) and modeled (red) data at the four wave stations inside Pohang New Port (W2, W3, W4, and W5) during the period of the wave event selected for BC from 05:30 on the 26 to 21:30 on 27 April 2009. Reasonable agreements are observed between the observational and modeled data, supporting the model validation.

A similar comparison between the modeled and observational data was carried out for the selected event case in AC. In Figure 14, the observed and modeled wave conditions in W1 are plotted for the period of the wave event selected for AC, from 07:00 on the 22 to 21:00 on 23 September 2019. Similar to the event case in BC, the wave conditions in W1 were nicely matched between the model and observation due to the proximity of the location of W1 to the open boundary. It was shown that the wave height increased to become the maximum ($H_{m0} \sim 4.8$ m) at 19:00 on 22 September 2019 and then gradually decreased to ~ 2.5 m at 21:00 on the 23rd in W1. The wave period generally increased from ~ 8.5 s to ~ 11.0 s, and the D_p value fluctuated between 30° and 60° , showing that the waves generally approached from NE in W1 during the wave event.

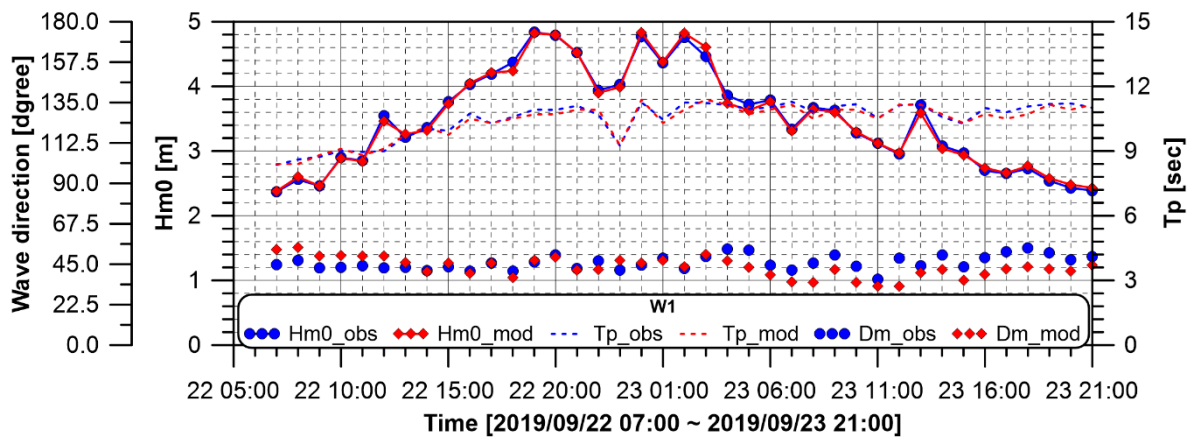


Figure 14. Comparison of wave conditions (H_{m0} , T_p , and D_p) between the observational (blue) and modeled (red) data in W1 during the period of the wave event selected for AC from 07:00 on the 22nd to 21:00 on 23 September 2019 (37 h). It is noted that the modeled data matched well with the observational data due to the proximity of W1 to the open boundary, as shown in the computational domain (Figure 4b).

Figure 15 compares the modeled wave heights with the observed data at the four wave stations (W2, W3, W4, and W5) inside Pohang New Port during the wave event selected for AC. It shows that the pattern of wave height time variation during the event was successfully generated by the model, although the errors estimated from the wave height were not improved compared to those in BC, as they were ~19.2%, 17.1%, 31.3%, and 19.2% for W2, W3, W4, and W5 respectively. The higher error range in AC was likely due to the lower magnitude of the observed H_{m0} , which would increase the error for the same deviation between the model and observation data.

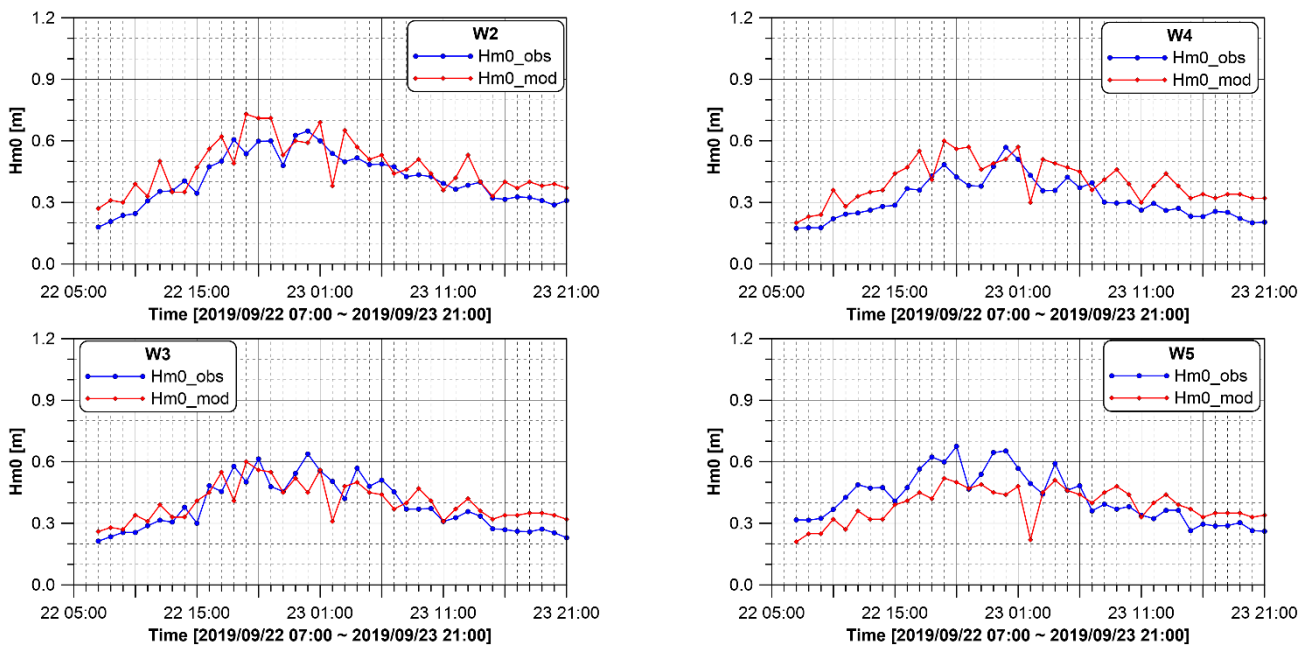


Figure 15. Comparison of wave height (H_{m0}) between the observational (blue) and modeled (red) data at the four wave stations inside Pohang New Port (W2, W3, W4, and W5) during the period of the wave event selected for AC from 05:00 on the 22 to 21:00 on 23 September 2019. Reasonable agreements are observed between the observational and modeled data, supporting the model validation.

Once the BOUSS-2D model was validated, the next step was to analyze the course of wave propagation to understand how the wave energy was reduced inside Pohang New Port through a comparison between BC and AC. In Figures 16 and 17, the contours of wave heights during the periods of the two wave events selected for BC and AC are compared. The contours are captured as a snapshot of the wave field at the time when the H_{m0} value became the maximum for each event, as shown in Figures 12 and 14. That is, in the case of BC, Figure 16 shows the field of wave heights at 15:30 on 26 April 2009 when the H_{m0} value became the maximum, 3.35 m (Figure 14). Similarly, the wave height field is contoured in Figure 17 at 19:00 on 22 September 2019, as it is the time when the H_{m0} value became the maximum (4.84 m) during the wave event selected for AC. The input wave conditions for the two cases were based on the observations at corresponding times. The wave period was similar between the two cases, as the T_p value was 11.0 s and 10.9 s for BC and AC, respectively. The wave direction was N35.0°E for BC and N46.3°E for AC, as they were propagating in the NNE–NE directions. Along the open boundary that was rotated 40° in the NE direction (Figure 4a), the incident wave direction was nearly normal to the boundary in both BC and AC (with a deviation of 5°–6°), indicating there were no significant discrepancies in terms of the input wave propagation direction between the two cases.

Both of the figures effectively compare the pattern of wave reduction inside Pohang New Port between the two cases. In BC (Figure 16), the isolines of the wave height became parallel to the port entrance where the narrow navigation channel is connected to the inside of the port. At the port entrance, the H_{m0} value was ~2.0 m (marked in a red rectangle in Figure 16), indicating that the H_{m0} value was reduced by ~40% from the input wave height at the outer open boundary (3.35 m). Once the waves entered the port, the wave height was rapidly reduced due to the combined effects of refraction and diffraction around the slits and other harbor structures, with H_{m0} varying from ~2.0 m to ~0.3 m. The wave height was observed to be 0.3 m inside the slit where the wave stations W4 and W5 were located (marked in a blue rectangle). It is noted, however, that the H_{m0} value was increased to 0.9 and 0.7 at the locations of wave stations W2 and W4, which was likely because the reflected waves were interfered with at the wall of the slits to increase the H_{m0} value to higher than that calculated off the walls.

In Figure 17, the H_{m0} isolines are contoured for the wave event selected for AC, which occurred at 19:00 on 22 September 2019. Compared to the case of BC, the detached breakwater was constructed near W1, blocking the waves. Behind the breakwater, therefore, H_{m0} was rapidly reduced, and the reduction rate was greater than that in BC. For example, the H_{m0} value became ~2.0 m near the entrance of Pohang New Port (marked in a red rectangle), and the reduction rate was 59% considering that the input wave height on the boundary was 4.84 m in AC, which was ~19% greater than that in BC. In addition, in AC (Figure 17), the red rectangle that marks the isoline position of $H_{m0} = 2.0$ m is located ~0.2 km further offshore compared to that in BC (compare with Figure 16), indicating that the wave heights inside the port would become lower than those in BC, assuming that the pattern of H_{m0} reduction inside the port would be same between the two cases, which was also confirmed from a comparison of the observed and modeled wave heights between BC and AC in W2, W3, W4, and W5, as shown in Figures 13 and 15.

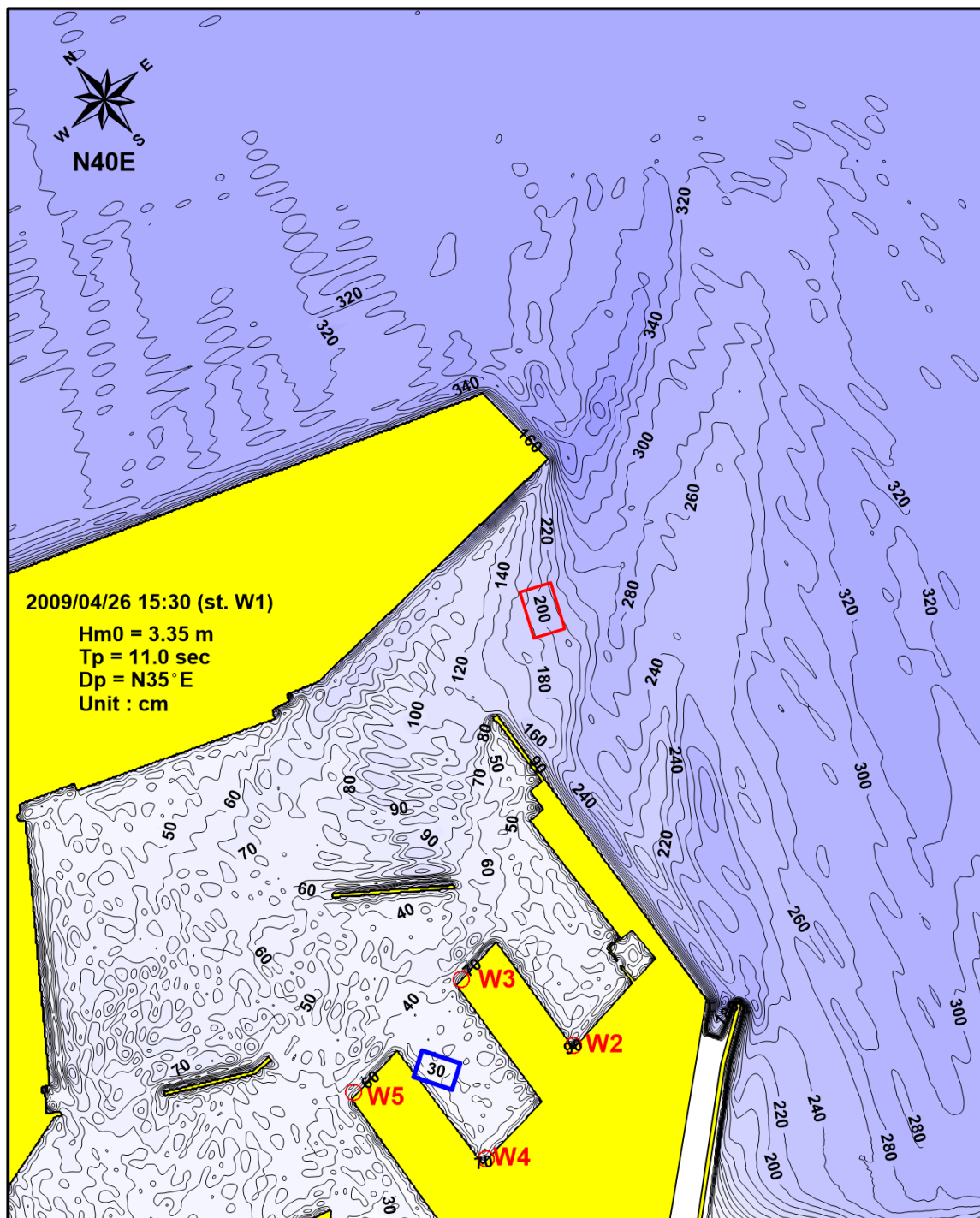


Figure 16. Contours of wave height isolines at 15:30 on 26 April 2009 when the H_{m0} value became maximum during the 39 h of the simulation time shown in Figure 12, in the case of BC. The input H_{m0} was 3.35 m at the open boundary, which was reduced to 2.0 m (40% reduction) near the entrance of Pohang New Port (marked in a red rectangle) and to 0.3 m inside the slit near W4 and W5 (marked in a blue rectangle).

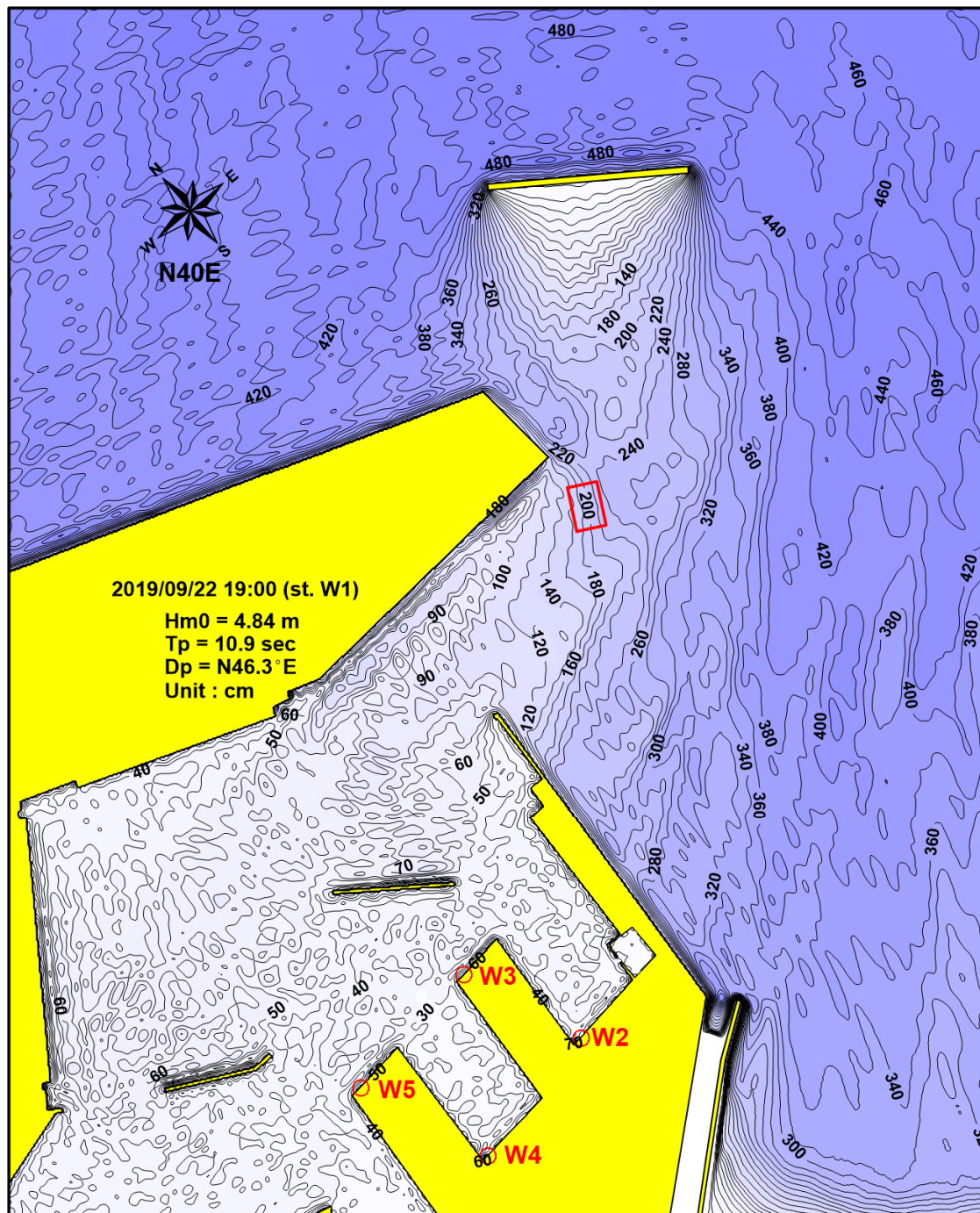


Figure 17. Contours of wave height isolines at 19:00 on 22 September 2019 when H_{m0} became maximum during the 39 h of the simulation time shown in Figure 16, in the case of AC. The input H_{m0} was 4.84 m at the open boundary, which was reduced to 2.0 m (59% reduction) near the entrance of Pohang New Port (marked in a red rectangle). It is also noted that the location of the 2.0 m H_{m0} isoline was slightly outside the port entrance compared to that in BC (Figure 16).

Figures 16 and 17 show the model that simulated the wave propagation patterns using the input conditions based on the observational data, and the input wave directions on the open boundary were similar between BC and AC, as they were $N35.0^\circ E$ and $N46.3^\circ E$, respectively. Therefore, the impact of wave directional change on the wave pattern inside Pohang New Port could not be examined using these model results, although it was observed from the observational data, as shown in Figures 8 and 9. In Figure 18, the

two additional cases that were tested for BC by assuming extreme cases in the wave propagation direction are shown. It is noted that most of the measured D_p values in W1 ranged between N15.0°E and N55.0°E in the case of AC, as shown in Figure 9. In Figure 18, therefore, the results of two model runs are shown with D_p set as N15.0°E (Figure 18a) and N55.0°E (Figure 18b), as they represent the extreme wave directions for NNE and NE waves, respectively. Except for the wave direction, the other input wave conditions were the same as those given for the case of BC in Figure 16. The results of these two extreme cases in Figure 18 could help us to understand the different patterns in the wave energy reduction rate inside Pohang New Port, according to the changes in D_p in W1, as observed in Figure 8 in the case of BC. In the extreme NNE case ($D_p = \text{N}15.0^\circ\text{E}$), the propagating waves outside the port mainly passed by the entrance of the port, and only the diffracted waves could enter the port, which increased the wave height reduction near the port entrance (Figure 18a). For example, the H_{m0} value was as high as 2.0 m just outside the port entrance, but it was reduced to 1.0 m just inside the port, as the distance between the two positions was only ~0.5 km (marked with two red rectangles). The high wave reduction rate near the port entrance meant that H_{m0} ranged from 0.2 to 0.7 m inside the port, and the estimated wave height reduction rate ($R_{W(model)} = \frac{H_{m0}[\text{inside PNP}]}{H_{m0}[\text{open boundary}]}$) was 5–20%. On the contrary, in the extreme NE case ($D_p = \text{N}55.0^\circ\text{E}$) shown in Figure 18b, the wave reduction near the port entrance was less severe compared to that in Figure 18a, as shown in the two marked red rectangles (the H_{m0} value was reduced from 2.0 m to 1.4 m for ~0.5 km). Therefore, the H_{m0} value inside the port was also higher compared to those in Figure 18a, with a range of 0.4–1.2 m in the areas, providing $R_{W(model)} = 12\text{--}35\%$ inside the port.

Figure 19 shows the model results of the two extreme wave directions that were tested for AC as well. That is, the other wave conditions were identical to those used in Figure 17, except that D_p was set as N15.0°E (N55.0°E), which represented an example of extreme conditions of NNE (NE) waves, as shown in Figure 19a (Figure 19b). Similar to the cases in BC, the wave propagation pattern inside Pohang New Port was affected by the different D_p input conditions at the open boundary, regardless of the existence of the detached breakwater. When D_p was N15.0°E, the H_{m0} value was significantly reduced in the lee area of the breakwater, as it was ~4.6 m offshore of the breakwater but decreased to ~2.0 m just outside the port, as shown in Figure 19a (marked with a red rectangle). The waves were then diffracted near the entrance of the port, where strong H_{m0} reduction occurred for the waves entering the port, as the H_{m0} value was reduced to ~1.0 m just inside the port (marked with a red rectangle). The range of H_{m0} was then 0.2–0.7 m inside the port, leading to $R_{W(model)} = 5\text{--}15\%$ inside the port. In the case of extreme NE waves ($D_p = \text{N}55.0^\circ\text{E}$ in Figure 19b), the waves approached the port from the NE direction, meaning the detached breakwater became less effective in reducing the wave height. For example, the H_{m0} value was reduced from ~2.0 m to ~1.4 m (marked in the red rectangles in Figure 19b) for the similar distance marked in Figure 19a. As a result, the H_{m0} value became higher inside the port, compared to that of D_p with N15.0°E, with the H_{m0} range of 0.4–1.2 m inside the port, providing $R_{W(model)}$ of 8–25% (Figure 19b). The impact of wave direction in the case of AC is further discussed in Section 4.

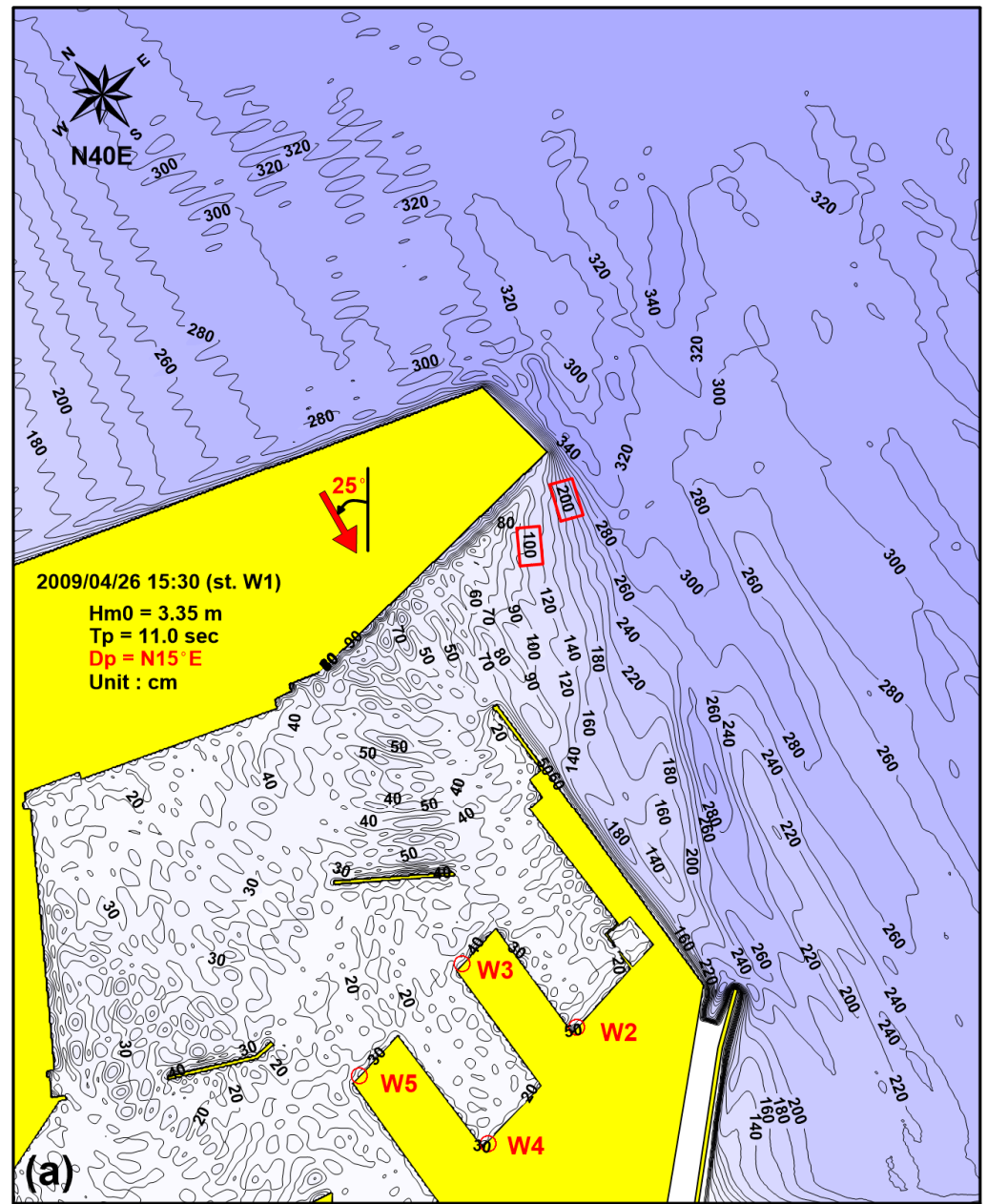


Figure 18. Cont.

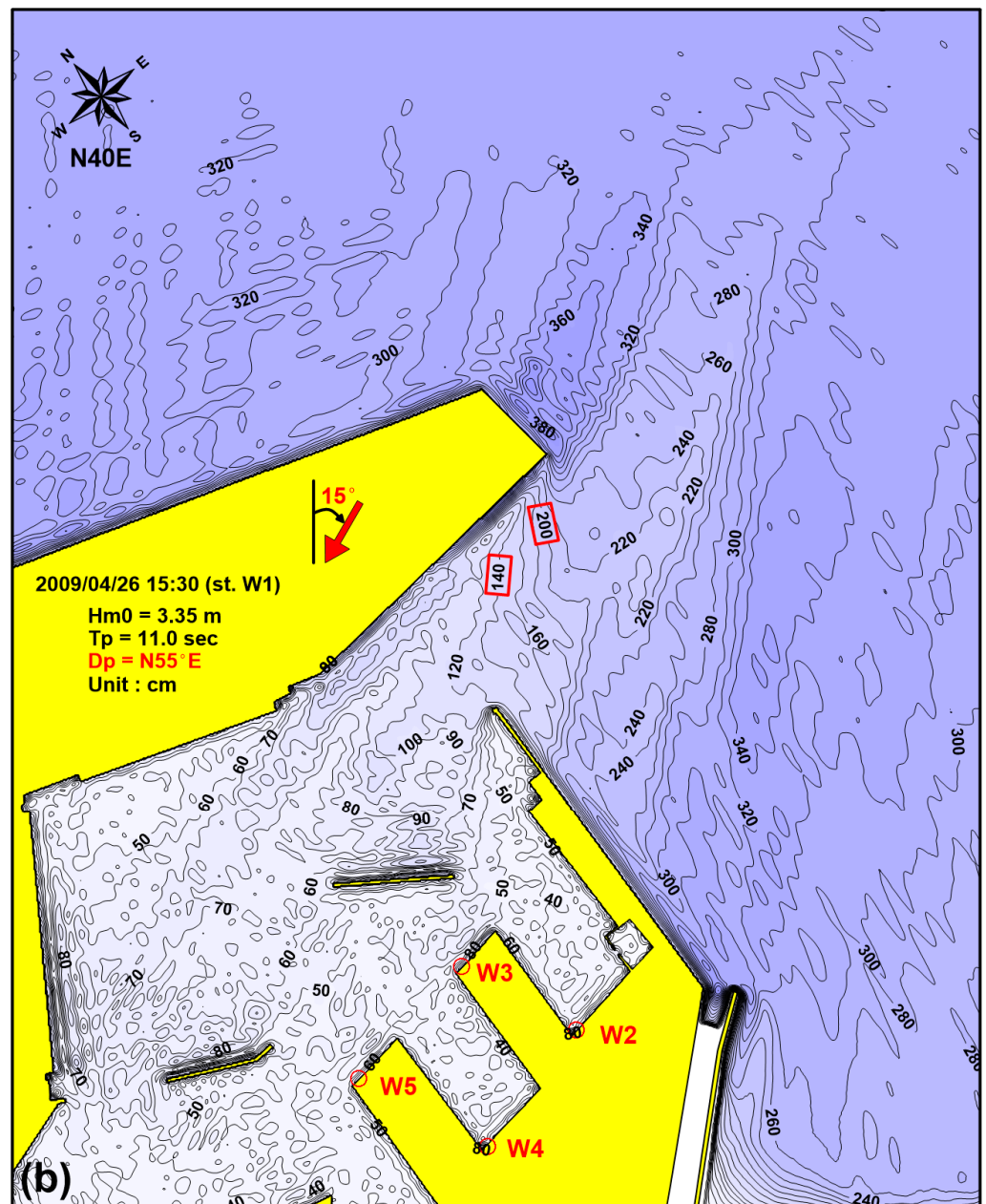


Figure 18. (a) Contours of wave height isolines in the case of BC. The model conditions were the same with those in Figure 16, except that D_p , the input wave direction along the outer open boundary, was set as $N15.0^\circ E$ as an example of extreme conditions that represented NNE waves; (b) the same as (a), except that D_p was set as $N55.0^\circ E$ as for an example of extreme conditions that represented NE waves. In the case of the extreme NE waves ($N55.0^\circ E$), the waves could enter into the port easily compared to the case of $N15.0^\circ E$.

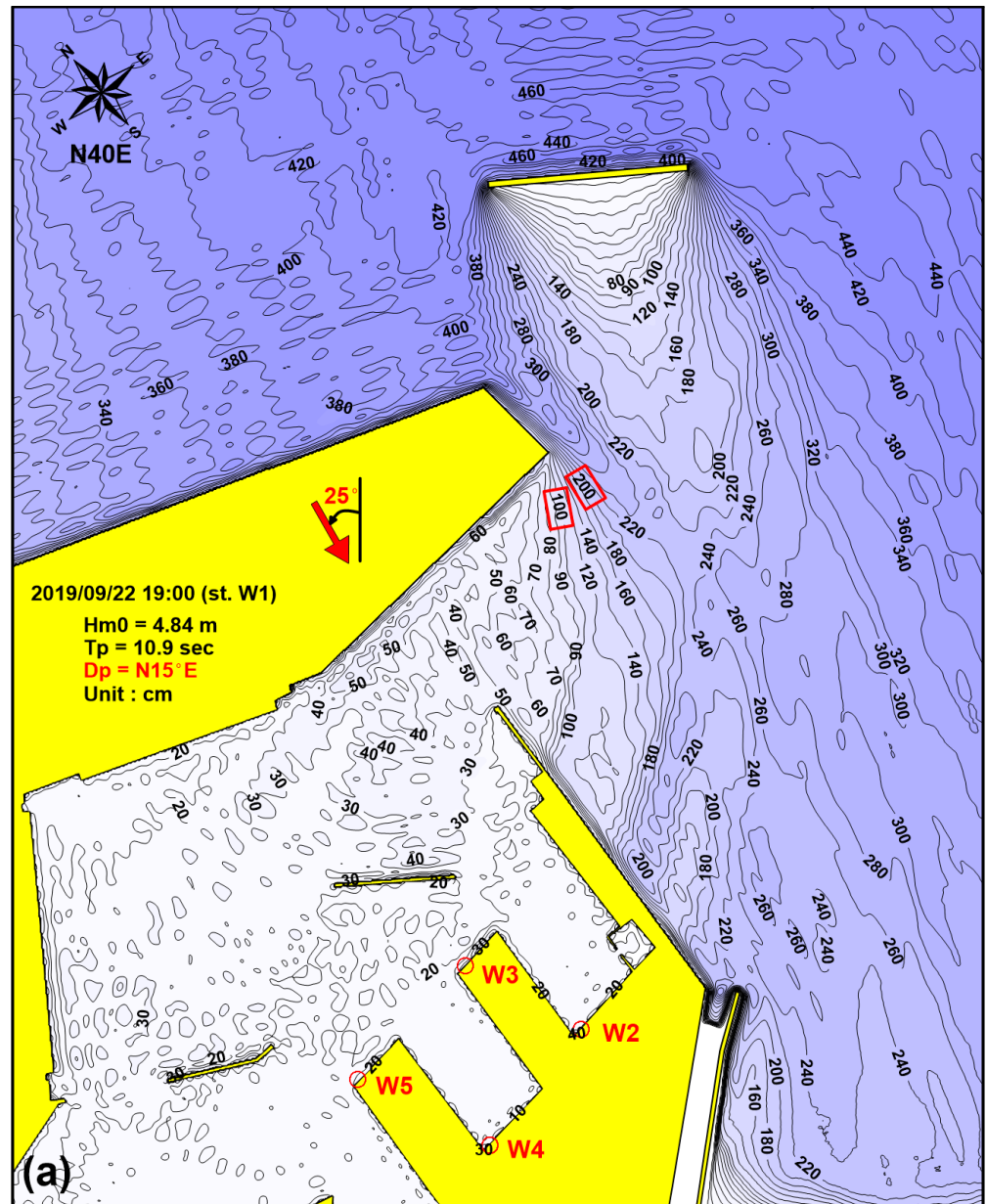


Figure 19. Cont.

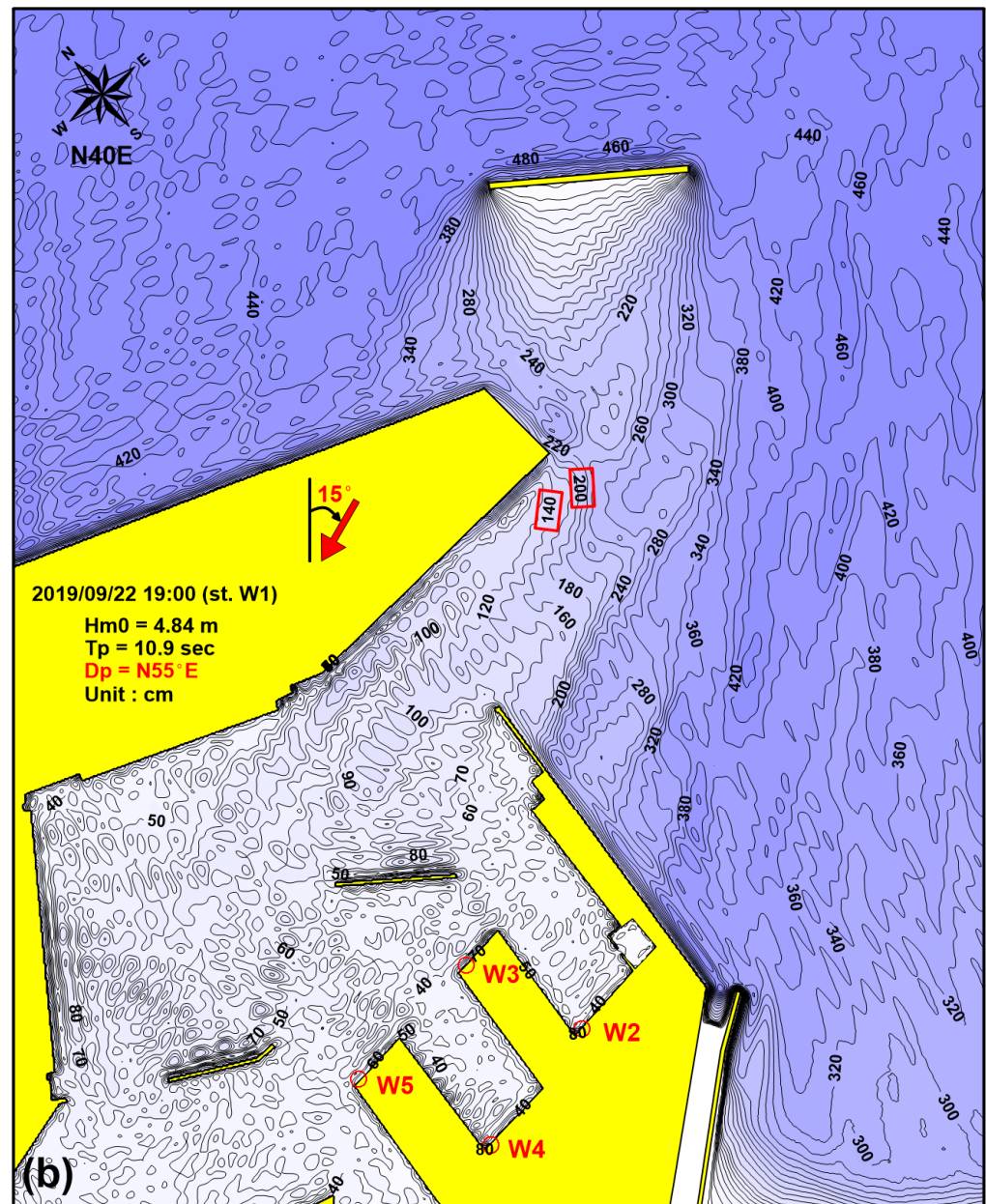


Figure 19. (a) Contours of wave height isolines in the case of AC. The model conditions were the same with those in Figure 17, except that D_p , the input wave direction along the outer open boundary, was set as $N15.0^\circ E$ as an example of extreme conditions that represented NNE waves; (b) the same as (a), except that D_p was set as $N55.0^\circ E$ as an example of extreme conditions that represented NE waves. In the case of the extreme NE waves ($N55.0^\circ E$), the waves could enter into the port easily compared to the case of $N15.0^\circ E$. When compared to the results in BC (Figure 18), wave height reduction occurred more effectively inside the port due to the detached breakwater.

4. Discussion

One of the most significant results of the present study was that the wave height reduction inside Pohang New Port was affected by the propagating wave directions that approached the detached breakwater. For example, in all of the wave stations inside the port, $R_{W\#}$ increased with increasing D_p . The close correlation between $R_{W\#}$ was observed in both BC and AC, as shown in Figures 8 and 9. However, the magnitude of $R_{W\#}$ became lower in AC. Figure 20 shows the comparison of the scatter plots of R_{W3} in terms of D_p between BC and AC. The distribution of the wave reduction rate was compared in W3

because it was located closest to the entrance of the port; thus, the impact of the wave propagation direction could be distinct in this station. The figure shows that R_{W3} increased with an increasing D_p value in both BC and AC. However, the magnitude of R_{W3} ranged from 0.12 to 0.40 in BC, but the magnitude was reduced by ~40% in AC, as R_{W3} ranged from 0.05 to 0.15. The lower magnitude of R_{W3} in AC indicates that the wave energy was effectively reduced inside the port, confirming the effect of the detached breakwater in securing the tranquility of the port.

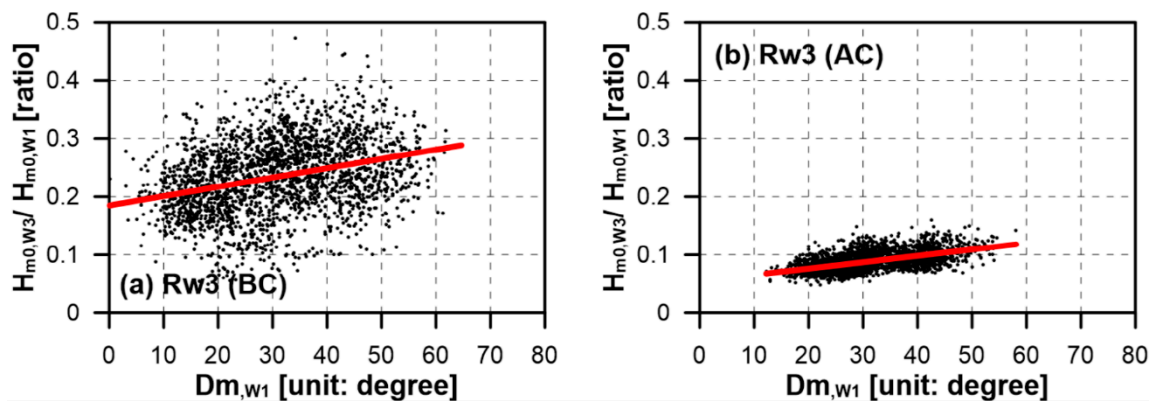


Figure 20. Comparison of the scatter plots of R_{W3} (the wave height reduction rate based on observation data) in terms of D_p in W1, (a) BC and (b) AC. The red line in each panel shows the linear regression calculated for each data set. The lower R_{W3} magnitude in AC indicates that the wave energy was effectively reduced inside the port, confirming the effect of the detached breakwater in securing the tranquility of the port.

Regardless of the observation of the significantly lower values of $R_{W\#}$ in AC, the result in Figure 20b indicates that the reduction in the wave height inside Pohang New Port became less effective even with the protection provided by the detached breakwater if the wave propagation direction increased (i.e., changed from NNE to NE). The cause for this was investigated using the BOUSS-2D model, which is displayed in Figure 19, showing that the wave heights were higher in the lee of the breakwater and also in the areas near the port entrance, as well as inside the port when the waves approached in the extreme NE direction (N55°E), which raised a question—“is the construction of a detached breakwater, as shown in Figure 1c, sufficient to reduce the wave energy in securing the tranquility inside the port for the waves approaching in all directions?” To find the answer, we needed to account for the fact that the eastern end of the breakwater was located near the western end of the navigation channel (see Figure 4b). From the engineering aspect, therefore, it was not practical to extend the breakwater further to the SE because the detached breakwater would then block the navigation channel. An alternative option would be to place another detached breakwater further SE, avoiding the navigation channel. However, this second option would not be effective either, considering that the extreme NE waves would approach in the N55.0°E direction, and thus, the new detached breakwater may be useless in blocking the waves propagating to the port entrance. Therefore, alternative options to construct additional engineering measures may not be practical, unless unavoidable.

The next step to find an answer to the question would be a statistical approach. From the results in Figure 9, it was shown that the magnitude of $R_{W\#}$ of the waves with D_p values greater than N55°E was mostly not higher than 0.15 at the wave stations located inside the port (W2–W5). In addition, as described in Section 1, the targeted maximum wave height to maintain the desired harbor tranquility inside the port was proposed as 0.3 m [13]. Therefore, considering that the maximum $R_{W\#}$ of the waves with D_p values greater than N55°E would be 0.15 for AC, the maximum H_{m0} value in W1 that would enable the tranquility inside the port to be maintained can be calculated as $0.3/0.15 = 2.0$ m.

Based on the wave measurements in W1 during the whole period of AC, in total, there was only 1 h in which the observed waves had D_p values greater than $N55^\circ E$ and H_{m0} values greater than 2 m. As this number is too small compared to the total period of wave measurement of 278 days in AC, the criteria for the extreme NE direction could be extended to $N50^\circ E$ and even to $N45^\circ E$. In these cases, however, the time in which the D_p value was greater than $N55^\circ E$ and the H_{m0} value was greater than 2 m was only 11 and 33 h, respectively, indicating that the probability of waves with heights that could be greater than 0.3 m inside the port because they approached from the extreme NE directions was $\sim 0.0\%$ ($>N55^\circ E$), and it would only become 0.2% ($>N50^\circ E$) and 0.5% ($>N55^\circ E$) if the criteria for the extreme NE direction were extended. Therefore, it can be concluded that the detached breakwater located in the current position was sufficient to protect the port by maintaining its tranquility with the targeted wave height, and no further secondary engineering structures would then be required. This recommendation provided to elevate the effectiveness of the detached breakwater could be determined based on the amount of observational data measured in both periods in BC and AC. Without these wave measurements, the model results could lead to overestimation or underestimation in evaluating the effect of the breakwater. Although this result was only found in this specific case, it can also provide an insight for future studies in planning/operating ports under similar environments in which unexpected extreme cases should be carefully considered, and these extremes may need to be evaluated from the sufficient data sets observed in the field.

5. Conclusions

In this study, observational and numerical experiments were conducted to investigate the effect of the detached breakwater on reducing the wave energy inside Pohang New Port in terms of the wave parameters and specifically, the wave propagation direction. The reason for selecting the wave direction as a primary controlling factor was to examine whether the position of the detached breakwater was appropriate in reducing the wave energy inside the port for the waves that approached in all practical directions. If not, it may have been necessary to consider placing additional structure(s) to secure the tranquility inside the port. For this purpose, wave data were measured before (BC) and after (AC) the detached breakwater was constructed at multiple stations inside and outside the port. In addition, the BOUSS-2D model based on Boussinesq-type equations was employed to investigate the effect of the detached breakwater on the wave propagation pattern around the breakwater and inside the port.

The observational results show that the wave energy (the ratio of H_{m0} inside and outside Pohang New Port) significantly decreased inside the port in AC compared to that in BC, although the wave height condition was generally higher outside the port (near the detached breakwater) in AC, which confirmed the effect of the breakwater. The reduction in the wave energy was observed in all wave propagation directions measured outside the port; however, the reduction rates inside the port showed that the effectiveness of the breakwater decreased as the wave direction changed from NNE to NE. The causes for the difference in the detached breakwater's effect depending on wave directions were investigated based on the model results, which made it possible to investigate the wave propagation pattern around the breakwater. In the case of BC, the model results showed that more wave energy could be transferred inside the port without severe transformation when the waves approached in the NE direction, which could be difficult for the waves approaching in the NNE direction as the waves mostly passed by the entrance of the port. In the case of the AC model runs, the detached breakwater could effectively block the waves that approached in both the NNE and NE directions, resulting in significantly enhanced wave reduction rates inside the port. In the extreme case of NE waves (e.g., wave direction = $N55.0^\circ E$) however, the wave energy increased inside the port regardless of the blocking caused by the breakwater, which might have required the consideration of additional engineering measures to secure the port tranquility. However, placing a

secondary detached breakwater would not be practical because the location of the current breakwater is too close to the navigational channel, meaning that further extension of the existing detached breakwater could block the channel itself. Further investigation based on the observational data showed that the probability of the wave height inside the port exceeding 0.3 m (the target wave height to maintain the tranquility inside the port) was only 0.2–0.5% when the waves approached in the extreme NE direction, indicating that no secondary structures might be necessary and that the existing detached breakwater would be enough to secure tranquility inside Pohang New Port.

Author Contributions: Conceptualization, K.H.R., W.M.J. and Y.S.C.; methodology, K.H.R., J.-E.O., and W.-D.B.; investigation, K.H.R., W.M.J., J.-E.O. and Y.S.C.; data curation, K.H.R. and W.-D.B.; supervision, W.M.J. and Y.S.C.; visualization, K.H.R. and J.-E.O.; writing—original draft preparation, K.H.R. and Y.S.C.; writing—review and editing, W.M.J. and Y.S.C.; funding acquisition, W.M.J. All authors have read and agreed to the published version of the manuscript.

Funding: This research was funded by the Korea Institute of Ocean Science and Technology (KIOST), grant number PEA0032, and the Ministry of Oceans and Fisheries, grant number PG52810.

Institutional Review Board Statement: Not applicable.

Informed Consent Statement: Not applicable.

Conflicts of Interest: The authors declare no conflict of interest.

References

- Oh, J.-E. *A Data-Based Downtime Forecasting Model in a Harbor: Application to Pohang New Port*; Seoul National University: Seoul, Korea, 2017.
- PIANC. *Criteria for Movements of Moored Ships in Harbours: A Practical Guide*; Permanent International Association of Navigation Congresses, Permanent Technical Committee, Working Group (PIANC) General Secretariat: Brussels, Belgium, 1995.
- Kankal, M.; Yükses, Ö. Artificial neural network approach for assessing harbor tranquility: The case of Trabzon Yacht Harbor, Turkey. *Appl. Ocean. Res.* **2012**, *38*, 23–31. [[CrossRef](#)]
- Moon, S.; Lee, J.; Kwon, S.; Song, H. Analysis of Harbor Tranquility due to Port Expansion. *J. Navig. Port Res.* **2019**, *43*, 320–327.
- Panigrahi, J.K.; Padhy, C.; Murty, A. Inner harbour wave agitation using boussinesq wave model. *Int. J. Nav. Archit. Ocean. Eng.* **2015**, *7*, 70–86. [[CrossRef](#)]
- Kankal, M.; Yükses, Ö.; Kömürçü, M.; Akpınar, A.; Önsoy, H. Physical and Numerical Modeling of Harbor Oscillations: A Case Study in Ünye Harbor, Turkey. *ENE* **2010**, *7*, 8.
- González-Marco, D.; Sierra, J.P.; de Ybarra, O.F.; Sánchez-Arcilla, A. Implications of long waves in harbor management: The Gijón port case study. *Ocean. Coast. Manag.* **2008**, *51*, 180–201. [[CrossRef](#)]
- Bellotti, G.; Franco, L. Measurement of long waves at the harbor of Marina di Carrara, Italy. *Ocean. Dyn.* **2011**, *61*, 2051–2059. [[CrossRef](#)]
- Kwak, M.S.; Jeong, W.M.; Kobayashi, N. A case study on harbor oscillations by infragravity waves. *Coast. Eng. Proc.* **2020**, *36*, 1–6. [[CrossRef](#)]
- Sakakibara, S.; Kubo, M. Characteristics of low-frequency motions of ships moored inside ports and harbors on the basis of field observations. *Mar. Struct.* **2008**, *21*, 196–223. [[CrossRef](#)]
- López, M.; Iglesias, G. Long wave effects on a vessel at berth. *Appl. Ocean. Res.* **2014**, *47*, 63–72. [[CrossRef](#)]
- Jeong, W.-M.; Ryu, K.-H.; Baek, W.-D.; Choi, H.-J. Downtime analysis for Pohang New Harbor through long-term investigation of waves and winds. *J. Korean Soc. Coast. Ocean. Eng.* **2011**, *23*, 226–235. [[CrossRef](#)]
- MOF. *Field Investigation Report for Swell Analysis and Improvement Measure Making of Downtime in Pohang New Harbor*; Ministry of Oceans and Fisheries: Pohang, Korea, 2010. (In Korean)
- MOF. *Report on Pohang New Port Swell Improvement Feasibility Test for Basic Plan*; Ministry of Oceans and Fisheries: Pohang, Korea, 2012. (In Korean)
- Ssangyong Engineering & Construction Co., L., Seoul, Korea. Personal communication, 2019. (In Korean).
- Ssangyong Engineering & Construction Co., L., Seoul, Korea. Personal communication, 2020. (In Korean).
- Ryu, K.H.; Jeong, W.M.; Kwon, J.; Chang, Y.S.; Baek, W.-D.; Kim, W.G. Evaluation of Harbour Tranquility Improvement in Pohang New Port by Detached Breakwater. *J. Korean Soc. Coast. Ocean. Eng.* **2020**, *32*, 230–241. [[CrossRef](#)]
- Kumar, P. Spectral wave modeling of tsunami waves in Pohang New Harbor (South Korea) and Paradip Port (India). *Ocean. Dyn.* **2020**, *70*, 1515–1530.
- Hanson, H.; Kraus, N.C. Shoreline response to a single transmissive detached breakwater. *Coast. Eng.* **1990**, 2034–2046.
- Vicinanza, D.; Lauro, E.D.; Contestabile, P.; Gisonni, C.; Lara, J.L.; Losada, I.J. Review of innovative harbor breakwaters for wave-energy conversion. *J. Waterw. Port Coast. Ocean. Eng.* **2019**, *145*, 03119001. [[CrossRef](#)]

21. Elchahal, G.; Younes, R.; Lafon, P. Optimization of coastal structures: Application on detached breakwaters in ports. *Ocean. Eng.* **2013**, *63*, 35–43. [[CrossRef](#)]
22. Zhang, Y.; Zhao, X.; Geng, J.; Tao, L. A novel concept for reducing wave reflection from OWC structures with application of harbor agitation mitigation/coastal protection: Theoretical investigations. *Ocean. Eng.* **2021**, *242*, 110075. [[CrossRef](#)]
23. Oh, J.-E.; Jeong, W.-M.; Ryu, K.-H.; Park, J.-Y.; Chang, Y.-S. Monitoring of Recovery Process at Yeongildae Beach, South Korea, Using a Video System. *Appl. Sci.* **2021**, *11*, 10195. [[CrossRef](#)]
24. Marino, M.; Rabionet, I.C.; Musumeci, R.E. Measuring free surface elevation of shoaling waves with pressure transducers. *Cont. Shelf Res.* **2022**, *245*, 104803. [[CrossRef](#)]
25. Nwogu, O.G.; Demirebilek, Z. *BOUSS-2D: A Boussinesq Wave Model for Coastal Regions and Harbors*; Engineer Research and Development Center Vicksburg Ms Coastal and Hydraulicslab: Vicksburg, MS, USA, 2001.
26. Peregrine, D.M. Long waves on a beach. *J. Fluid Mech.* **1967**, *27*, 815–827. [[CrossRef](#)]
27. Nwogu, O. Alternative form of Boussinesq equations for nearshore wave propagation. *J. Waterw. Port Coast. Ocean. Eng.* **1993**, *119*, 618–638. [[CrossRef](#)]
28. Wei, G.; Kirby, J.T.; Grilli, S.T.; Subramanya, R. A fully nonlinear Boussinesq model for surface waves. Part 1. Highly nonlinear unsteady waves. *J. Fluid Mech.* **1995**, *294*, 71–92. [[CrossRef](#)]
29. Nwogu, O.G. Numerical prediction of breaking waves and currents with a Boussinesq model. *Coast. Eng.* **1996**, 4807–4820.